Developing an Optimization Algorithm for Solving Economic Dispatch Problem in Microgrids

Mohammad Lotfiakbarabadi

Submitted to the
Institute of Graduate Studies and Research
in partial fulfillment of the requirements for the degree of

Master of Science
in
Electrical and Electronic Engineering

Eastern Mediterranean University
September 2021
Gazimağusa, North Cyprus

Approval of the Institute of Graduate Studies and Research

Prof. Dr. Ali Hakan Ulusoy
Director

I certify that this thesis satisfies all the requirements as a thesis for the degree of Master of Science in Electrical and Electronic Engineering.

Assoc. Prof. Dr. Rasime Uyguroğlu
Chair, Department of Electrical and Electronic Engineering

We certify that we have read this thesis and that in our opinion it is fully adequate in scope and quality as a thesis for the degree of Master of Science in Electrical and Electronic Engineering.

Assoc. Prof. Dr. Reza Sirjani
Supervisor

Examining Committee

1. Prof. Dr. Osman Kükrer

2. Assoc. Prof. Dr. Reza Sirjani

3. Asst. Prof. Dr. Moein Jazayeri

ABSTRACT

In the power system, one of the remarkably popular and fundamental optimization problems is economic power dispatch. Economic dispatch in a classical form contains only thermal generators without considering network security constraints. However, other forms of this problem like economic emission dispatch are gaining more importance since minimization of emission is predominant from the environmental point of view. Moreover, integrating renewable sources comes with challenges due to the stochastic nature of them. In this study, a multi-objective algorithm is developed to deal with the problem of economic emission power dispatch integrated with solar, wind, and small-hydro unit. Lognormal, Weibull and Gumbel distribution for predicting the accessible power of solar, small hydro, and wind power is utilized respectively. For the goal of the study, some of the traditional generators are replaced in the structure of the IEEE 30-bus network, with different renewable units of energy. Voltage limitation, capacities of the transmission line, prohibited areas of operation for the thermal generator plants, and restriction of the system are also considered. Multi-objective real coded non-dominated sorting genetic algorithm II is enforced to the problem of this study while incorporating a decent procedure of handling system restrictions, constraint domination, to meet the system limitations. Results are looked over in parts and discussed. The proposed method was then compared with two previous methods from another study to exhibit the robustness of the suggested technique. Results have been found to be significant. R-NSGA-II can reduce the cost up to $4,853.04 a year compared with the SMODE-SF method and $1,795.8 a year compared to the MOEA/D-SF method.

Keywords: Multi-objective optimization, Economic emission dispatch, renewable energy, stochastic modelling, microgrid.

ÖZ

Güç sisteminde son derece popüler ve temel optimizasyon problemlerinden biri ekonomik güç sevkidir. Klasik formdaki ekonomik sevk, ağ güvenliği kısıtlamalarını dikkate almadan yalnızca termal jeneratör içermektedir. Ancak bu sorunun ekonomik emisyon sevkiyatı gibi diğer biçimleri, emisyonun en aza indirilmesinin çevresel açıdan baskın olması nedeniyle daha fazla önem kazanmaktadır. Ayrıca, Yenilenebilir kaynakları şebekeye entegre etmek, stokastik doğası nedeniyle zorluklarla birlikte gelmektedir. Bu çalışmada, güneş, rüzgar ve küçük hidro ünite ile entegre ekonomik emisyon gücü sevk problemini ele almak için çok amaçlı bir algoritma geliştirilmiştir. Lognormal, Weibull ve Gumbel dağılımı güneş, küçük hidro ve rüzgar enerjisinin erişilebilir gücünü tahmin etmek için sırasıyla kullanılmaktadır. Çalışmanın amacı doğrultusunda, IEEE-30 test şebekesinin yapısında olan bazı geleneksel jenaratörler, farklı yenilenebilir enerji birimleriyle değiştirilmiştir. Gerilim sınırlaması, iletim hattının kapasiteleri, termik jeneratör tesisleri için yasak çalışma alanları ve sistemin kısıtlanması da göz önünde bulundurulmaktadır. Çok amaçlı gerçek kodlu baskın olmayan sıralama genetik algoritması II, bu çalışmanın problemine uygulanırken, sistem kısıtlamalarını karşılamak için kısıtlama derecesini ele almak için iyi bir prosedür içermektedir. Sonuçlar parçalar halinde incelenip, tartışılmaktadır. Önerilen yöntem daha sonra sunulan tekniğin sağlamlığını göstermek için başka bir çalışmada uygulanan iki yöntemle karşılaştırılmıştır. Sonuçlar anlamlı bulunmuştur. R-NSGA-II, maliyeti SMODE-SF yöntemine göre, yılda 4,853,04 dolara, MOEA / D-SF yöntemine göre ise yılda 1,795,8 dolara kadar düşürülebilmektedir.

Anahtar Kelimeler: Çok amaçlı optimizasyon, Ekonomik emisyon dağıtımı,

yenilenebilir enerji, stokastik modelleme, mikro şebeke.

DEDICATION

Dedicated to Maria, the blessing of my life.

ACKNOWLEDGMENT

Paramount, I thank, the one and only, the supreme, the comforter, the one that can't be conceived, nor described fully, Allah, from the bottom of my soul and with all my heart, for having my back in all dimensions and aspects, and it will never be enough.

Next, I thank my dear supervisor, Assoc. Prof. Dr. Reza Sirjani, who guided me and has borne with me and my ignorance, throughout my years of studying master. May God bless you and your loved ones.

In the end, I thank my family, my loved ones, my friends, my co-workers, and everyone who made me kept going, for their unconditional help and energy. May God bless you and your loved ones too.

TABLE OF CONTENTS

LIST OF TABLES

LIST OF FIGURES

LIST OF SYMBOLS AND ABBREVIATIONS

$f_G(G_s)$	Probability of solar irradiance Gs
$f_q(Q_w)$	Probability of river flow rate Qw
$f_v(v)$	Probability of the speed of the wind (v)
G_s	Solar irradiance in w/m^2
g_w	Direct fee coefficient related to the wind plant
h_s	Direct fee coefficient related to the solar unit
K_{Ps}	Penalty cost coefficient related to the solar plant underestimation
K_{Psh}	Penalty cost coefficient regarded with the hybrid plant
K_{Pw}	Penalty fee coefficient related to the wind plant underestimation power
K_{Rs}	Reserve cost coefficient related to the solar plant overestimation
K_{Rsh}	Reserve cost coefficient related to the hybrid plant
K_{Rw}	Reserve fee coefficient related to the wind plant overestimation power
m_h	Direct fee coefficient related to the hybrid unit
ms	Mutation probability
P_{hr}	Graded output power related to the small hydro plant
P_{loss}	Actual power loss in the system
P_{sav}	Actual accessible power related to the solar unit

P_{shav}	Actual accessible power related to the hybrid unit
P_{sr}	Graded output power of the solar unit
P_{ss}	Scheduled power related to the solar unit
P_{ssh}	Scheduled power related to the hybrid unit
P_{TGi}	Power output from the i^{th} thermal plant
P_{wav}	Actual accessible power related to the wind unit
p_{wr}	Graded output power of a wind plant
P_{ws}	Scheduled power related to the wind unit
Q_w	River flow rate in m^3/s
SF	Superiority of feasible answers
SPH	A hybrid system, combination of a solar plant and a small hydro (which run according to flow of the river) plant
TG/T_G	Thermal power plant/generator
WG/W_G	Wind plant/generator
α,β	Weibull PDF's scale parameter and shape parameter respectively
λ,γ	Gumbel PDF's location specification and scale value respectively
μ,δ	Lognormal PDF's mean parameter and standard deviation respectively
CH	Constraint handling technique
DEED	Dynamic economic emission dispatch
ED	Economic dispatch

EED	Economic-environmental/emission dispatch
HV	Hypervolume indicator
ISO	Independent system agent/operator
MOEA/D	Decomposition based method for multi objective evolutionary algorithm
MOEED	Multi objective economic emission dispatch
PDF	Probability density function
POZ	Prohibited/forbidden operating zone
PV	Photovoltaic
R-NSGA-II	Real coded non-dominated sorting genetic algorithm II
SBX	Simulated binary crossover
SMODE	Summation based method for multi-objective differential evolution technique
VD	Voltage deviation aggregation of load buses in the system

Chapter 1

INTRODUCTION

1.1 Context of the Study

1.1.1 Definition of a Microgrid

Environmental concerns like global warming are becoming more eminent each day. Means of diminishing carbon emission are the objectives of industries and governments, as they are trying to find techniques for solving this problem. Coal-powered units or central steam are getting old since distributed generation is the trend and motivation towards it is increasing. Penetration of different renewable sources can be enabled by a distributed generation where the location of consumer is closer to these sources of renewable energy [1], [2]. Nevertheless, implementing renewable generation has its own downsides and comes with different challenges.

Lasseter [3], [4] introduced the microgrids concept as a way of implementing dispersed energy resources in a supervised and safe manner. A group of interlinked distributed energy resources and loads within distinctly established electrical borderlines that performs as an individual tractable unit vis a vis with the grid is often defined as a microgrid. Operation of a microgrid can have two cases of grid-connected or islanded-mode since they can connect to the grid or disconnect from it to enable this feature [5].

Microgrids became more popular to the customers and stakeholders since their benefits are not limited to providing energy only, but they can also diminish gas emissions of

a greenhouse, lessened peak loading, improvement of quality of the power, and stability of services [6], [7].

1.1.2 Hydro Power Stations

Hydro power is a traditional renewable source of energy between conventional generations. Hydro power is more clean and cheaper when compared to thermal power plants. Almost 20% of the world's electricity is coming from hydro power. Small hydro power in vast distribution is valued as a source of generation particularly in remote areas. The weather and the water flow of the river, affect power generation of hydro power that is run-of-the-river type. It's obvious that the power coming from these types is stochastic and intractable. Although, dams can be treated as storage to introduce control in these types of hydro power [8].

1.1.3 Wind and Solar Power

One of the most propitious origins of clean energy is wind power which has been developing in the last few decades. Since wind power doesn't need any gas and does not yield any carbon emissions, the installation growth rate of wind power has been boosted globally. Although, the cost of investment is higher than hydro power or traditional power plants which work with fossil fuel. The nature of wind energy sources is stochastic and for that, operating hours in a year are low. Hence, on average and in most cases, 1MW electricity produced by wind power has more cost comparing to the traditional power plants [8].

Solar energy is also a promising clean source of energy since photovoltaic panels can produce electricity directly from the sun and sunshine is free of charge. However, the cost to invest in photovoltaic panels is high, even higher than wind power, considering the efficiency of PV panels is about 10% with the tools and technologies we currently have [8].

1.1.4 Unit Commitment

Unit commitment determines which generators to use, at which times, and at what production rate in the power system while having the data to forecast the load [9]. Minimizing the production cost is the aim of optimization while deciding on the scheduling and in doing that, all constraints of the system must be satisfied. There are limitations of the power units as well as the transmission lines in any network. Different constraint in each network can be boundaries of generation, ramp rate limits, etc., that needs to be considered while meeting the electricity demand.

1.1.5 Economic Dispatch

Economic dispatch is the determination of the minimum possible cost for the required power from each committed power plant [10]. In other words, learning the ideal output of a collection of power units in order to meet the network request at the lowest viable charge while satisfying the operation and transmission restrictions.

In a power network, utilities are in charge of installing and planning new power units based on the predicted load growth in the network. A reliable system should have the accessible generation competence to be more than the peak load and the needed reserve edge. The Schedule of the unit commitment is made in advance by the system operator, according to the predicted load profiles and maintenance schedules of generators. The least ON/OFF time of the generator, costs of generator startup and operation, reserve requirements, etc., are to be considered for the ON/OFF schedule of the generating plants. For a certain time period, say an hour, normally multiple generators are scheduled to be ON. The attribute and class of generators can be different. The total electricity demand for each hour must be satisfied by the system operator with making the schedule for the generation dispatch of all generators. Typically, the important matter of dispatching a generation plant is the fuel cost. Plants with less cost of fuel

are dispatched to produce more electricity. This is a basic straightforward economic principle for generation dispatch. Although, implementing that simple principle is in fact hard, since attributes of power generations are not linear and generation output is in a non-linear relationship with fuel consumption [8].

1.2 Optimization

The system operator realizes that when a system has the number of generating units more than one, the cost of the fuel is different for each generation's schedule of each unit. This happens because of different attributes in each generating unit and the fuel usage is not a linear function in relation to the power output and it is dependent on its fuel usage curve and where the operating point is. The fuel consumption of each generator is different for a specified electricity load. If supplying the load can be done with one generator only, the one with the least fuel usage will be selected while if more generators are needed, different combinations of generators are an option which results in different fuel usage and costs. The economical schedule is achieved by selecting the combination that results in the lowest possible cost. Obviously, the system operator can calculate every option and figure out which combination will result in the least possible cost. However, this method may not be useful in a system with a huge number of generators as it can take forever to calculate all the possibilities. To figure out this obstacle, optimization methods can be utilized and that is the objective of the economic operation of the power system [8].

1.3 Problem Definition

It is reasonable to say that the economic emission dispatch problem has a fundamental significance in any power system. Reduction of emission degree and the whole cost of generation while satisfying the demand, is the preeminent issue of economic-emission load dispatch. Since there are high amounts of uncertainty in renewable generation,

this problem comes with a lot of challenges.

High penetration of divergent origins of renewable energy adds to the instability of the system because of the stochastic nature of them. Having implemented higher than one class of renewable energy source like wind, solar or hydro will increase the uncertainty of the system even more. Since prediction error is the main relation of these uncertainties, reducing the instability of the network is of importance and can be achieved by studying different scenarios for each renewable type that exists in the system.

Furthermore, an optimization method is needed to compute the optimal output for economic emission dispatch since there can be too many numbers of generation units in the system to be enumerated one by one. Also, diminishing cost or emission is a single objective problem but to reduce both of them at the same time, the problem becomes non-convex. Hence, there are more than one solution to the problem and specific methods must be used in order to extract those answers.

1.4 Thesis Objectives

This study will aim to:

1. Develop an efficient, reliable, cost and emission-effective economic dispatch algorithm that can handle multi-objective optimization.
2. Study of forecasting renewable energy sources of different types and implementing them in the system.
3. Satisfy many system constraints and network securities during optimization.
4. Compare the results of the developed algorithm with two other different algorithms to assess the robustness of the method.

1.5 Thesis Framework

The thesis is organized as:

Chapter 1 serves as an introduction to this thesis defining a research background, problems and expressing the goals of this work.

Chapter 2 gives out a more in-depth literature review laying out developments and trends in the economic emission load dispatch problem. Different methods of optimization with different constraints are reviewed and key concepts and ideas behind the problem are stated.

Chapter 3 formally presents the detailed methodology that is practiced in this study. It states the proposed R-NSGA-II and its elitist characteristics alongside the genetic operators that are incorporated within. It also includes the explanation of different methods which are used to forecast renewable energy sources and their implementation in the standard IEEE 30 bus system. Furthermore, it gives out the methods of extracting the best-compromised solution integrated with the algorithm.

Chapter 4 presents the outcomes of the simulation for the developed algorithm on the standard IEEE 30 bus network combined with renewable energy sources. It also shows the compared results with two other different algorithms to assess the accomplishments of the suggested algorithm.

Chapter 5 summarizes and concludes the thesis and the presented study. It suggests the possible future work that can be implemented and studied.

Chapter 2

LITERATURE REVIEW

2.1 Overview

In EED, the main objective is to minimize the total price of generation as well as the emission degree while at the same time, fulfilling electricity demand from the power unit. Climatic contamination is mostly caused by thermal power units which produce Sulphur dioxide, a toxic gas, represented with SO_2 and other similar gases like Nitrogen oxide and Carbon dioxide represented with NOx and CO_2 respectively [11].

There can be three different ways of solving EED according to Ref. [12-14]. Firstly, the problem is considered to be a single objective, only containing emission, since in many countries environmental laws impose a carbon tax, hence practicing emission control is of more importance. Secondly, mixing emission and cost both into a single objective optimization and reducing them at the same time by considering different weights [15]. And thirdly, with a multi-objective optimization which has different separate functions, in this case, cost and emission [11].

A solution to the EED problem falls into two parts. Economic dispatch (ED) and emission optimization. In the first section, optimal scheduling of generator units is performed to reduce electricity demand while in the second section, the same task is performed to diminish the amount of greenhouse gas. Several methods have been used to achieve these tasks while satisfying problem constraints concerning generator

capacity and limits, security, and network operation.

2.2 Background and Previous Researches

Adarsh et al. [16] used the bat algorithm, a variant of swarm intelligence technique combined with chaotic sequences for tuning and controlling the parameters resulting in convergence and diversity enhancement.

Jayabarathi et al. [17] implemented the hybrid gray wolf algorithm to solve the ED problem with a single objective. The hybrid part acquired operators of crossover and mutation for enhancing the algorithm.

The introduction of the multi-fuel option, as well as the valve-point effect, was done in Ref. [18] for solving ED problems.

Delshad et al. [14] utilized backtracking search algorithm (BSA) to overcome the ED issue following Ref. [18], containing various feed options and valve-point effect. Then adding more complexity to the ED problem by considering POZs and generators ramp-up and ramp-down, since BSA is promoted to solve very non-convex functions.

Implementing emission into the formula requires multi-objective optimization. Secui [19] used an approach known as the weighted sum, with a newly altered artificial bee colony algorithm. Aside from the valve-point effect, other restrictions like transmission losses, POZ, and ramp-rate boundaries have been considered to improve the mathematical model.

Gjorgiev et al. [20] used a similar approach of weighted sum with the genetic algorithm and applied a modified version of dynamic normalization as a penalty function to

improve the method. Also, for constraint violation calculation, a penalization method was used based on membership functions.

Zhang et al. [21] implemented a modern multi-objective optimization parallel with particle swarm known as the bare-bone optimization algorithm. A good feature is that it does not require the user to customize the parameter control due to the existence of a strategy that updates the particles.

Rao et al. [22] performed multi-objective optimization of EED problems with a new approach named adaptive clonal selection algorithm. The principle of clonal selection was used to implement the artificial immune system behavior.

So far, in all of these articles, thermal generators have been incorporated solely. The following literature has dealt with EED problems having wind energy implemented in them alongside thermal generators.

Mondal et al. [23] enforced the gravitational search technique to solve the MOEED problem with the incorporation of wind energy sources at weak load busses by measuring their L-index value. A penalty factor was implemented to consider underestimation, reserve, and overestimation price of wind power in stochastic mode.

Yao et al. [24] implemented both a carbon tax and stochastic wind power in the EED model and then Quantum-inspired particle swarm optimization was adopted to solve the issue which showed the speed of the convergence to be faster and the search ability to be stronger.

Jadhav et al. [25] reached a better convergence and accuracy by applying Gbest guided artificial bee colony on ED problem having wind-thermal structure and considering generator ramp limits, POZs, and valve-point effect.

All literature in Ref. [23-25] converted the EED problem from a multi-objective into a single objective. Hence, the non-dominated group of solutions of the multi-objective problem could not be used to make decisions for the dispatch strategy.

Abul'Wafa et al. [26] considered valve-point effect along with reserve and penalty price of the stochastic wind energy in MOEED problem and applied the second version of NSGA with a controlled elitist approach (CNSGA-II).

Ghasemi et al. [27] implemented a 2m-point practical model for the uncertainty in wind power while approaching the MOEED problem by using honey bee mating optimization combined with two trained neural networks to overcome the local optima convergence.

Qu et al. [28] used the summation-based differential evolution technique in a multi-objective form and considering the uncertainty of wind to be a constraint of the system while applying superiority of feasible solution to comply with the constraints.

Zhu et al. [29] adopted a multi-objective evolutionary algorithm based on decomposition and treated uncertainty of the wind power as a constraint while implementing a penalty to the objective function for overcoming constraints of the system.

Azizipanah-Abarghooee et al. [30] implemented a 2m point estimation method to solve the MOEED problem with overestimation and underestimation of the wind power while achieving an optimal solution for a set of non-dominated by employing a modified teaching-learning algorithm.

Khan et al. [31] solved EED with thermal and solar power by applying the particle swarm method while converting the multi-objective function to a single objective function.

Kheshti et al. [32] introduced Lightning Flash Algorithm, a new evolutionary algorithm for solving non-convex ED problems in large scales considering valve-point effects and multiple fuel options.

Not much literature can be traced regarding the model of solar, thermal, and wind power system and this is true for a combination of wind and hydro energy sources. Hence, more research is required.

Reddy et al. [33] performed single objective optimization considering wind, thermal and solar power in the system and approaching the scheduling problem with the best-fit evaluation of participation factors.

Reddy [34] executed optimal scheduling of a hybrid system (wind-solar-thermal) together with battery storage by using a two-point estimate method and genetic algorithm.

Biswas et al. [35] used the success history-based adaptation technique coupled with

separate probability density functions as well as underestimation and overestimation of the renewable energy sources to solve the optimal flow problem.

Liu et al. [36] integrated the improved gradient descent with an evolutionary algorithm to solve the DED problem contain small hydro and wind energy sources, Gumbel and Weibull probability density functions were used respectively to represent random behavior of mentioned energy sources.

Salkuti et al. [37] executed particle swarm optimization to compute single and multi-objective EED problems by adding thermal-wind-solar power in the system and implemented prohibited operating zones and valve point loading effect as well.

Yalcinoz et al. [38] used improved particle swarm optimization to solve the multi-objective EED problem while implementing wind energy in the system and considering generator limitations being valve point effect, ramp restrictions with transmission losses as well as prohibited operating zones.

Up to this point, a combination of wind, small-hydro, solar, and thermal power plants has not been mentioned. The following articles have been demonstrated the combination of these energy sources all together while considering different density function for predicting the behavior of them.

Li et al. [39] performed optimization of DEED incorporated with renewable energy units (wind, solar and hydro) by approaching the multi-objective problem with moth-flame optimization technique while using Beta, Gumbel, and Weibull distribution for simulation of uncertainty in solar, hydro, and wind power, respectively.

Biswas et al. [40] applied both method differential evolution being decomposition-based and summation based algorithm in the multi-objective problem of environmental economic dispatch and considering solar, wind, and small hydro power network while simulating the stochastic behavior of them with Lognormal, Weibull, and Gumbel distribution, respectively.

Sarda et al. [41] used the cuckoo search algorithm to achieve optimal active–reactive power dispatch as well as flower pollination algorithm while implementing small-hydro, wind, and solar power units in the network and predicting their uncertain behavior with Gumbel, Weibull, and Lognormal distribution, respectively.

Sulaiman et al. [42] solved the optimal power flow problem incorporated with stochastic units of solar, wind, and hydro while using barnacles mating optimizer which showed the effectiveness of the approach.

Pandya et al. [43] utilized the multi-verse optimizer to calculate multi-objective optimal power flow along with clean power sources like wind, solar, small hydro and applied Weibull, Lognormal and Gumbel distribution to forecast the behavior on these uncertain energy sources, respectively.

Abdullah et al. [44] solved the multi-objective problem of optimal power flow by proposing a method known as improved multi-objective multi-verse optimization and enhancing the algorithm by using non-dominated sorting and crowding distance while considering renewable energy sources.

This study suggests an approach having a multi-objective function implemented with

non-linearity and uncertainty to compute environmental economic dispatch containing various sources like wind, solar, thermal, and small hydro units.

Table 2.1. Summary of the methods along with key features and structure.

Method	Structure	Key feature	Ref.
Backtracking search algorithm	Thermal Plant	With Valve-point effects	[14]
Chaotic implementation of bat algorithm	Thermal Plant	With transmission losses	[16]
Grey wolf optimizer in hybrid form	Thermal Plant	Without transmission losses	[17]
Crisscross optimization algorithm	Thermal Plant	With multiple fuel options	[18]
Artificial bee colony algorithm with modification	Thermal Plant	With transmission losses	[19]
Classical genetic algorithm	Thermal and hydrothermal plants	With generator limit	[20]
Bare-bones multi-objective particle swarm optimization algorithm	Thermal Plant	Fuzzy membership function	[21]
Adaptive clonal selection method	Thermal Plant	With/without load uncertainty	[22]
Gravitational search algorithm	Thermal and wind plants	Weibull distribution	[23]
Quantum-inspired particle swarm optimization	Thermal and wind plants	Weibull distribution	[24]
Gbest guided artificial bee colony algorithm	Thermal and wind plants	Weibull distribution	[25]
Controlled elitist NSGA-II	Thermal, wind, and solar plants	Clearness index PDF	[26]
Honey bee mating optimization	Thermal and wind plants	Piecewise linear approximation	[27]

Summation based multi-objective differential evolution	Thermal and wind plants	Weibull distribution	[28]
Multi-objective evolutionary algorithm in a decomposition-based form	Thermal and wind plants	Weibull distribution	[29]
2m point estimated method	Thermal and wind plants	Piecewise linear approximation	[30]
Particle swarm optimization	Thermal and solar plants	Full radiation and clouds effect	[31]
Lightning flash algorithm	Thermal plant	New algorithm	[32]
Best-fit participation factor	Thermal, wind, and solar plants	Log-normal distribution	[33]
Genetic algorithm, Two-point estimate method	Thermal, wind, and solar plants	Weibull distribution	[34]
Success history-based adaptation technique	Thermal, wind, and solar plants	Log-normal distribution	[35]
Improved gradient descent with an evolutionary algorithm	Thermal, wind, and small hydro plants	Gumbel distribution	[36]
Particle swarm optimization	Thermal, wind, and small hydro plants	Weibull distribution	[37]
Improved multi-objective particle swarm optimization algorithm	Thermal and wind plants	Improved method	[38]
Multi-objective moth-flame optimization	Thermal, wind, solar and hydro plants	Beta distribution	[39]
MOEA/D and SMODE	Thermal, wind, solar, and small hydro plants	Gumbel distribution	[40]

Cuckoo search algorithm	Thermal, wind, solar, and small hydro plants	Log normal distribution	[41]
Barnacles mating optimizer	Thermal, wind, solar, and small hydro plants	Gumbel distribution	[42]
Multi verse optimizer	Thermal, wind, solar, and small hydro plants	Log normal distribution	[43]
Improved multi-objective multi-verse optimization	Thermal, wind, solar, and small hydro plants	Weibull distribution	[44]

Chapter 3

METHODOLOGY

3.1 Specification of the System

The main characteristics of the adjusted IEEE 30-bus network [40] can be seen in Table 3.1. The revised network's illustration can be seen in Fig. 3.1. Three thermal generators are connected to the system, one generator at bus number 1, another generator is at bus 2 and the last generator is at bus 8. A wind generator is supplying bus 5. A solar photovoltaic (SPV) plant is at bus 11.

Table 3.1. The essential features of the revised IEEE 30-bus system [40].

System characteristics	Amount	Details
Bus	30	Table A.1 (Appendix)
Branch	41	Table B.1 (Appendix)
Thermal generator ($T_{G1}; T_{G2}; T_{G3}$)	3	Bus numbers: 1 (swing), 2 and 8
Wind generator (WG)	1	Bus number: 5
Solar photovoltaic unit (SPV)	1	Bus number: 11
Solar unit + small-hydro ($SPVH$)	1	Bus number: 13
Control variable	11	Scheduled actual power of five generators: T_{G2}, T_{G3}, W_G, PV and PVH; voltage of bus for all six plants/generator
Corresponding load (P and Q)	-	283.4 MW , 126.2 $MVAr$
Acceptable load bus voltage range	24	0.95–1.10 (pu)

A run of river small-hydro power unit is considered so that there would be no need for storage in most cases [45]. A small-hydro has the potential of giving few megawatts as output power at best [45]. There comes the SPV unit, which is integrated with the small-hydro unit supplying bus 13 to improve the total output power. It is obvious that outputs of a solar plant, wind, and small-hydro units are variable dependent

and any amount of output shortage from them must be diminished by the spinning reserve. It can be seen in Table 3.1, that there are 11 variables of the system. All these variables should be optimized thus maintaining the economical and efficient operating of the system.

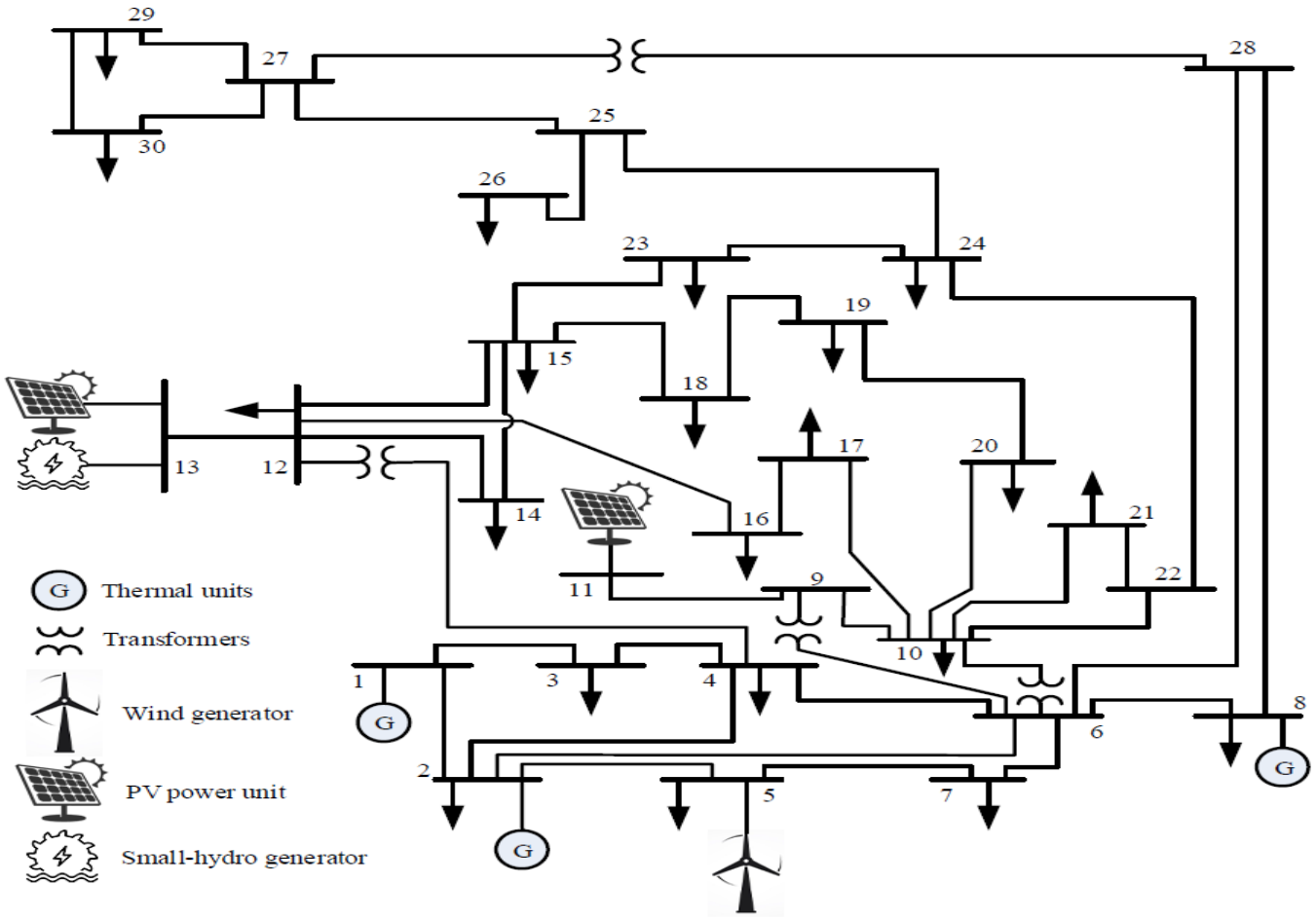

Figure 3.1. The revised IEEE structure with 30 bus having solar, small hydro and wind plants.

3.2 Thermal Generator Cost

Fuel price (in $/h) for the thermal plant comply with a quadratic curve that can be expressed as [35]:

$$C_{T0}(P_{TG}) = \sum_{i=1}^{N_{TG}} a_i + b_i P_{TGi} + c_i P_{TGi}^2 \tag{3.1}$$

where a_i, b_i, and c_i show the price coefficients of the i^{th} thermal plant P_{TGi}. And N_{TG} is the entire number of thermal plants in the system. This representation of the fuel price is simple but, in real-world cases, it becomes much more convoluted and nonlinear.

For instance, by considering the valve-point loading effect, due to the presence of stacking impacts of the valve point, the generation fuel cost function grows into non-convex with so many curls as it can be seen in Fig 3.2 [46]. To be more accurate, the increased charge due to the effects of steam i.e. valve-point is treated as [35]:

$$C_T(P_{TG}) = \sum_{i=1}^{N_{TG}} a_i + b_i P_{TGi} + c_i P_{TGi}^2 + \left| d_i \times \sin\left(e_i \times (P_{TGi}^{\min} - P_{TGi}) \right) \right| \tag{3.2}$$

where e_i and d_i are for considering the price coefficients of the valve-point effect. The lowest output of the i^{th} thermal plant when it's operating is $P_{TGi}^{\min}$. All of the price coefficients of thermal generators plants are provided in Table 3.2.

Table 3.2. Coefficients of thermal generators for cost and emission [40].

Gen	Bus	a	b	c	d	e	α	β	μ	ω	φ
T_{G1}	1	30	2	0.00375	18	0.037	4.091	-5.554	6.490	0.0002	6.667
T_{G2}	2	25	1.75	0.01750	16	0.038	2.543	-6.047	5.638	0.0005	3.333
T_{G2}	8	20	3.25	0.00834	12	0.045	5.326	-3.550	3.380	0.0020	2

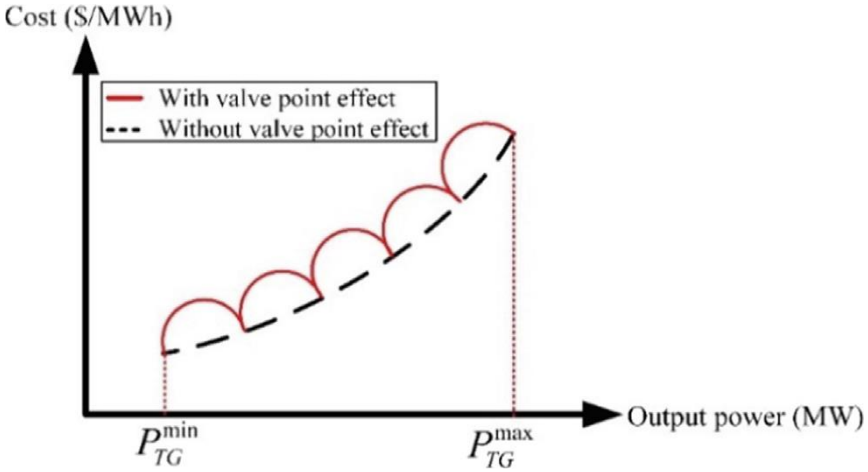

Figure 3.2. The output power with effects of valve point effect.

3.3 Price of Periodic and Stochastic Renewable Energy Plants

Integration of renewable plants into the power grid has difficulty due to the periodic and stochastic characteristics of nature. Generally, PV farms, wind farms, etc. are inherited by the non-public organization which endures a buy consensus with the independent system operator (ISO) for a specific volume of scheduled power. The ISO is responsible to diminish the shortage amount of the scheduled power if these renewable sources are insufficient or non-available. Thus, the spinning reserve must be kept if the demand occurs. This situation is termed as an overestimation of renewable sources like windfarm and solar-farm and it adds extra cost for the ISO. Conversely, a condition may occur when these renewable sources generate more power than the scheduled power which is called underestimation. In this case, the extra generated power can be wasted due to the non-utilization. So, the ISO must endure the penalty fee. Hence all fees of these renewable plants contain direct cost parallel to the scheduled power, overestimation fee on account of the spinning reserve, and penalty price owing to the underestimation.

The direct fee of the wind farm as an objective of the scheduled power can be shown as [40]:

$$\left(P_{ws}\right) = g_w P_{ws} \tag{3.3}$$

where g_w specify the direct fee coefficient of the wind plant. P_{ws} designates the scheduled power of the same unit.

Likewise, for the solar power unit, the direct fee related to the solar unit is [40]:

$$\left(P_{ss}\right) = h_s P_{ss} \tag{3.4}$$

where h_s indicates the direct price coefficient of the solar PV unit and P_{ss} specifies the scheduled power of the same unit.

There is a third hybrid power plant considered in this case study which is owned by a single non-public operator that contains a small-hydro power unit and a solar PV plant. The direct price coefficients for these plants are non-identical. The output of the small-hydro power plant differs in line with the movement speed of the river [47]. Nevertheless, because the volume of the small-hydro power unit is trivial in comparison with the requested load of the network, this source generally operates at maximum.

Direct price linked with the hybrid unit calculated as [40]:

$$C_{sh}(P_{ssh}) = C_{sh}(P_{ssh,s} + P_{ssh,h}) = h_s P_{ssh,s} + m_h P_{ssh,h} \tag{3.5}$$

where P_{ssh} indicates the scheduled output power from the hybrid plant, $P_{ssh,s}$ is the influence of solar unit and $P_{ssh,h}$ is the influence of small-hydro unit. The coefficient of direct price for the solar plant is h_s like the previous, and for the small-hydro unit,

the coefficient is m_h.

3.3.1 Stochastic Wind Power Price Computation

As discussed previously, owing to the stochastic essence of wind energy, the power output can be insufficient compared to what the scheduled amount is. If such a case occurs, ISO must have enough operating reserve to diminish the demand. The price of operating reserve for the wind plant can be computed as [35]:

$$C_{Rw}(P_{ws} - P_{wav}) = K_{Rw}(P_{ws} - P_{wav}) = K_{Rw}\int_{0}^{P_{ws}} (P_{ws} - p_w) f_w(p_w) d p_w \tag{3.6}$$

where the reserve price coefficient K_{Rw} is for the wind unit and the real power available from the same unit is P_{wav}. The probability density function (PDF) for the wind unit is represented by $f_w(p_w)$.

If underestimation happened in any case, the output power from the wind unit could be wasted due to the non-utilization. To utilize it, the output power of the normal generators must be reduced. A penalty price cost must be paid by the ISO if such a case arises. Charge of the penalty for the wind plant is formulated as [35]:

$$C_{Pw}(P_{wav} - P_{ws}) = K_{Pw}(P_{wav} - P_{ws}) = K_{Pw}\int_{P_{ws}}^{P_{wr}} (p_w - P_{ws}) f_w(p_w) dp_w \tag{3.7}$$

where penalty fee coefficient K_{Pw} is for the wind unit and calculated output power of the same unit is P_{wr}.

3.3.2 Stochastic Solar Power Price Computation

The method for calculating the over and underestimation of solar power is similar to the windfarm. Although, in windfarm, a well-known Weibull PDF is drawn, but for the solar radiation, lognormal PDF is mostly used [33, 48]. For ease of calculation, like the idea which is explained in [35, 49], penalty and reserve fees are formulated accordingly. Reserve fee of the PV unit for overestimation formulated as [35]:

$$C_{Rs}(P_{ss} - P_{sav}) = K_{Rs}(P_{ss} - P_{sav}) = K_{Rs} * f_s(P_{sav} < P_{ss}) * [P_{ss} - E(P_{sav} < P_{ss})] \quad (3.8)$$

where K_{Rs} is the coefficient of the reserve fee related to the solar power unit and P_{sav} is the actual accessible power for the same unit. The possibility of solar output deficit event is represented by $f_s(P_{sav} < P_{ss})$ and $E(P_{sav} < P_{ss})$ is the prediction of solar output power beneath P_{ss}.

For the opposite case of overestimating the solar unit cost, the penalty fee for underestimation is formulated as [35]:

$$C_{Ps}(P_{sav} - P_{ss}) = K_{Ps}(P_{sav} - P_{ss}) = K_{Ps} * f_s(P_{sav} > P_{ss}) * [E(P_{sav} > P_{ss}) - P_{ss}] \quad (3.9)$$

where K_{Ps} is the coefficient of the penalty fee for the solar unit. The likelihood of solar power surplus is represented by $f_s(P_{sav} > P_{ss})$ and the possibility of PV power exceeding P_{ss} is $E(P_{sav} > P_{ss})$.

3.3.3 Stochastic Hybrid Unit Price Computation

Massive facilities of hydro power have enormous pools, making them suitable sources of spinning reserve. However, because the capacity of small-hydro is tiny in comparison to network production and consumption, operating reserve size of it may not matter to the ISO. In actuality, penalty or reserve fees may not be applicable to the non-public agents of small-hydro plants at all. The 3rd production unit in our instance

is a hybrid system. It consists of a solar PV plant mixed with a small hydro plant. The small hydro plant's output is determined by the flow rate of the river, which is notorious to follow the Gumbel distribution [50, 51]. The PV power plant is now eligible for penalty and reserve cost, similar to the one described previously. We include penalty fees for underestimated and reserved fees for overestimated entire quantities of power output from the hybrid unit, for calculation purposes. This is due to the fact that the small hydro contributes around 10-20% only.

Subsequent Eq (3.8), overestimation reserve fee of the power from the hybrid unit is [40]:

$$C_{Rsh}(P_{ssh} - P_{shav}) = K_{Rsh}(P_{ssh} - P_{shav}) = K_{Rsh} * f_{sh}(P_{shav} < P_{ssh}) * [P_{ssh} - E(P_{shav} < P_{ssh})] \quad (3.10)$$

where the coefficient K_{Rsh} is for the reserve price of the hybrid plant, and the real available output power of the same plant is shown as P_{shav}. The possibility of the power shortage event of this hybrid unit is $f_{sh}(P_{shav} < P_{ssh})$ and $E(P_{shav} < P_{ssh})$ is the prediction of hybrid unit output power lower than P_{ssh}.

Following Eq (3.9), the underestimation penalty fee of the hybrid power output is [40]:

$$C_{Psh}(P_{shav} - P_{ssh}) = K_{Psh}(P_{shav} - P_{ssh}) = K_{Psh} * f_{sh}(P_{shav} > P_{ssh}) * [E(P_{shav} > P_{ssh}) - P_{ssh}] \quad (3.11)$$

where the coefficient of penalty fee in relation with the hybrid unit is K_{Psh}, the possibility of the hybrid unit power surplus is given by $f_{sh}(P_{shav} > P_{ssh})$. The prediction of hybrid unit output power exceeding P_{ssh} is $E(P_{shav} > P_{ssh})$.

3.3.4 Emission

Both atmosphere and environment are filled with noxious gases that are released from fossil-fueled thermal generators. The quantity of greenhouse gas emissions, like NO_x

as well as SO_x , etc., fluctuates with the amount of production power generated, coming from Eq (3.12). Emission (t/h) can be shown as [35]:

$$Emission, E_{Tot} = \sum_{i=1}^{N_{TG}} \left[(\varphi_i + \psi_i P_{TGi} + \omega_i P_{TGi}^2) \times 0.01 + \tau_i e^{(\zeta_i P_{TGi})} \right] \quad (3.12)$$

where φ_i, ψ_i, ω_i, τ_i and ζ_i are coefficients of emission related to the i_{th} thermal plant. All of the mentioned coefficients can be seen in Table 3.2.

3.4 Objectives of Optimization

In the EED problem, the intention is to minimize both production price as well as emission. To calculate the total price of generation, the cost of the thermal generators, as well as the direct price of the renewable power along with their reserve and penalty price, must be summed. Hence, the total price of 3 thermal generators, 1 wind generator, 1 solar generator, and 1 hybrid generator which is a combination of a small-hydro and a PV can be specified as the summation of Eq (3.2)-(3.11) [40]:

$$\begin{aligned} C_{Tot} &= C_T(P_{TG}) + [C_w(P_{ws}) + C_{Rw}(P_{ws} - P_{wav}) + C_{Pw}(P_{wav} - P_{ws})] \\ &+ [C_s(P_{ss}) + C_{Rs}(P_{ss} - P_{sav}) + C_{Ps}(P_{sav} - P_{ss})] \\ &+ [C_{sh}(P_{ssh}) + C_{Rsh}(P_{ssh} - P_{shav}) + C_{Psh}(P_{shav} - P_{ssh})] \end{aligned} \quad (3.13)$$

Objective function of multi-objective optimization [40]:

$$Minimize\ [C_{Tot}, E_{Tot}] \quad (3.14)$$

There exist many inequality and equality restrictions in the EED problem.

3.5 Equality Limitations

For immediate power balancing, equality constraints require that the generated real and reactive power be equal to all of the network's corresponding demands and losses [35].

$$P_{Gi} - P_{Di} - V_i \sum_{i=1}^{NB} V_j [G_{ij} \cos(\delta_{ij}) + B_{ij} \sin(\delta_{ij})] = 0 \qquad \forall i \in NB \tag{3.15}$$

$$Q_{Gi} - Q_{Di} - V_i \sum_{j=1}^{NB} V_j [G_{ij} \sin(\delta_{ij}) - B_{ij} \cos(\delta_{ij})] = 0 \qquad \forall i \in NB \tag{3.16}$$

where $\delta_{ij} = \delta_i - \delta_j$, represents the distinction in voltage gradient of bus i as well as bus j. Real load demand related with the bus i is P_{Di} and reactive load demand for the same bus is Q_{Di} while for the same bus, P_{Gi} and Q_{Gi} are real and reactive power generation respectively, from a conventional or renewable source. NB indicates overall busses in the system. The conductance being G_{ij} between bus i and j, and the susceptance being B_{ij} between bus i and j.

3.6 Inequality Limitations

In the EED problem, the inequality limitations consist of prohibited/forbidden operating zones (POZ) for thermal generators, operational limitation range of all generators in the system, and security limitations for busses as well as the transmission lines. In the Eq (3.17)-(3.20) limitations for the actual power production of the thermal unit, wind plant, solar generator, and hybrid unit are given, respectively, while Eq (3.21)-(3.24) specify the imaginary power limitations of the same generators with the same order.

Generator constrains for operational limitation range [40]:

$$P_{TGi}^{\min} \le P_{TGi} \le P_{TGi}^{\max} \qquad \forall i \in N_{TG} \tag{3.17}$$

$$P_{ws}^{\min} \le P_{ws} \le P_{ws}^{\max} \tag{3.18}$$

$$P_{ss}^{\min} \le P_{ss} \le P_{ss}^{\max} \tag{3.19}$$

$$P_{ssh}^{\min} \le P_{ssh} \le P_{ssh}^{\max} \tag{3.20}$$

$$Q_{TGi}^{\min} \le Q_{TGi} \le Q_{TGi}^{\max} \qquad \forall i \in N_{TG} \tag{3.21}$$

$$Q_{ws}^{\min} \le Q_{ws} \le Q_{ws}^{\max} \tag{3.22}$$

$$Q_{ss}^{\min} \le Q_{ss} \le Q_{ss}^{\max} \tag{3.23}$$

$$Q_{ssh}^{\min} \le Q_{ssh} \le Q_{ssh}^{\max} \tag{3.24}$$

Prohibited operating zones (POZ) are introduced to avoid discontinuity of the cost curve of thermal generators. Sometimes thermal generators can't operate in the whole range and this happens because of different reasons like shaft bare quivering, a flaw in the generator itself, or its attachments like boilers, pumps, etc. [25]. POZs can be represented as [40]:

$$P_{TGi}^{\min poz,j} < POZ_{TGi}^{j} < P_{TGi}^{\max poz,j} \tag{3.25}$$

where the lower bound and upper bound of the j^{th} POZ are $P_{TGi}^{\min poz,j}$ and $P_{TGi}^{\max poz,j}$ respectively for the i^{th} thermal unit.

System security constraints can be shown as [40]:

$$V_{Gi}^{\min} \le V_{Gi} \le V_{Gi}^{\max} \qquad \forall i \in NG \tag{3.26}$$

$$V_{Lp}^{\min} \le V_{Lp} \le V_{Lp}^{\max} \qquad \forall p \in NG \tag{3.27}$$

$$S_{lq} \le S_{lq}^{\max} \qquad \forall q \in nl \tag{3.28}$$

Limitations of the voltage for the generator buses are shown in Eq (3.26) and NG is the number of generators whether it is renewable or generator bus. Voltage limitations for the load buses are represented by Eq (3.27) while limitations of the line are specified in Eq (3.28). NL is the number of load busses in the system while nl is the value of transmission lines inside the system.

Out of the abovementioned different limitations, equality boundaries of balancing power are satisfied by default, when the convergence of power flow happens. MATPOWER [52] is used with applying the Newton-Raphson method for performing and calculating the power flow.

Generator bus voltages and generator real power (excluding slack bus) are automatically handled for their inequality constraints. Within their specified range, the optimization algorithm selects a feasible solution that contains sets of control variables. If a generator is within the POZs, the algorithm must not select that value for decision variables. In other words, the algorithm is only allowed to select the values which are not in the range of POZs. An appropriate handling technique for remaining inequality boundaries is a must so that the limitations of them are all held correctly.

Some parameters like power loss of the system shown in Eq (3.29) and Voltage deviation (VD) shown in Eq (3.30), which shows the quality of voltage in the system are considered. VD can be calculated by summing voltage deviations for all load buses in the system [53].

$$P_{loss} = \sum_{q=1}^{nl} G_{q(ij)} \left[V_i^2 + V_j^2 - 2V_i V_j \cos(\delta_{ij}) \right] \tag{3.29}$$

where, $\delta_{ij} = \delta_i - \delta_j$, represents voltage angle difference of buses *i* and *j* and $G_{q(ij)}$ is the transfer conductance related to branch *q* which connects bus *i* and bus *j*.

$$VD = \sum_{p=1}^{NL} \left| V_{Lp} - 1 \right| \tag{3.30}$$

3.7 Computing Uncertain Production of Renewable Power Sources

3.7.1 Distribution Probability of Power for Renewable Sources

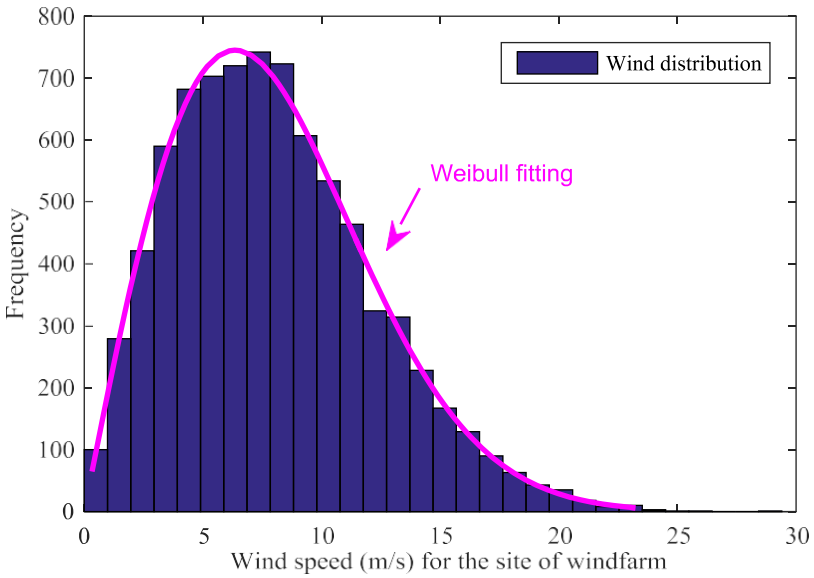

Figure 3.3. Distribution of the speed of the wind (8000 sample size) at bus 5.

For representing wind speed, Weibull PDF is mainly used [33-35]. Speed of the wind (v) m/s possibility is formulated as [35]:

$$f_v(v) = \left(\frac{\beta}{\alpha}\right)\left(\frac{v}{\alpha}\right)^{(\beta-1)} e^{-(v/\alpha)^{\beta}} \quad for \quad 0 < v < \infty \tag{3.31}$$

where α is the scale parameter and β is the shape of Weibull characteristics, respectively. Values for all PDF parameters can be seen in Table 3.3. These values are selected rationally with consideration of the capacity installed for power generation sources and most of them are the same as in Ref. [35]. It can be seen in Fig.3.3 the amount of sample size and the result after simulating Monte-Carlo cases [40].

Table 3.3. All parameters of PDF for probability modeling of renewable energy.

Wind plant at (bus 5)				Solar unit at (bus 11)		Hybrid unit solar combined with small hydro at (bus 13)		
Plant amount	Sum graded power, P_{wr}	Weibull characteristic		Graded power, P_{sr}	Lognormal characteristic	Solar plant graded power, P_{sr}	Lognormal characteristic	Small hydro graded power, P_{hr}	Gumbel characteristic
25	75 MW	$\alpha = 9$ $\beta = 2$		50 MW	$\mu = 5.2$ $\sigma = 0.6$	45 MW	$\mu = 5.0$ $\sigma = 0.6$	5 MW	$\lambda = 15$ $\gamma = 1.2$

For solar insolation distribution (G_s), lognormal PDF is used and it can specify the possibility of it as [35]:

$$f_G(G_s) = \frac{1}{G_s\sigma\sqrt{2\pi}} \exp\left\{\frac{-(\ln G_s - \mu)^2}{2\sigma^2}\right\} \qquad for \qquad G_s > 0 \tag{3.32}$$

Where μ is the mean and σ is the standard deviation of lognormal PDF.

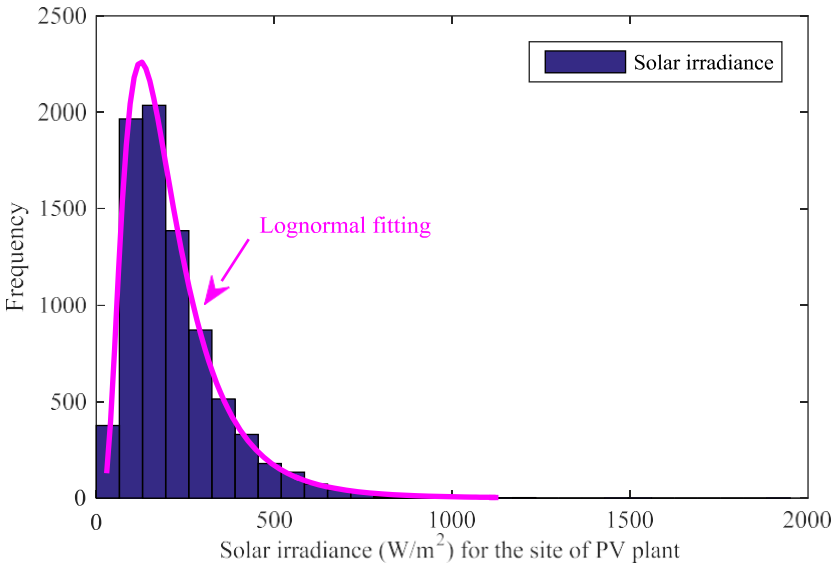

Figure 3.4. Distribution of solar irradiance of the PV plant (8000 samples) regarding bus number 11.

Distribution of Gumbel can represent the flow rate of river as [40]:

$$f_Q(Q_h) = \frac{1}{\gamma}\exp\left(\frac{Q_h - \lambda}{\gamma}\right)\exp\left[-\exp\left(\frac{Q_h - \lambda}{\gamma}\right)\right] \tag{3.33}$$

where λ is the location parameter, γ is the scale, and Q_h is the flow rate of the river.

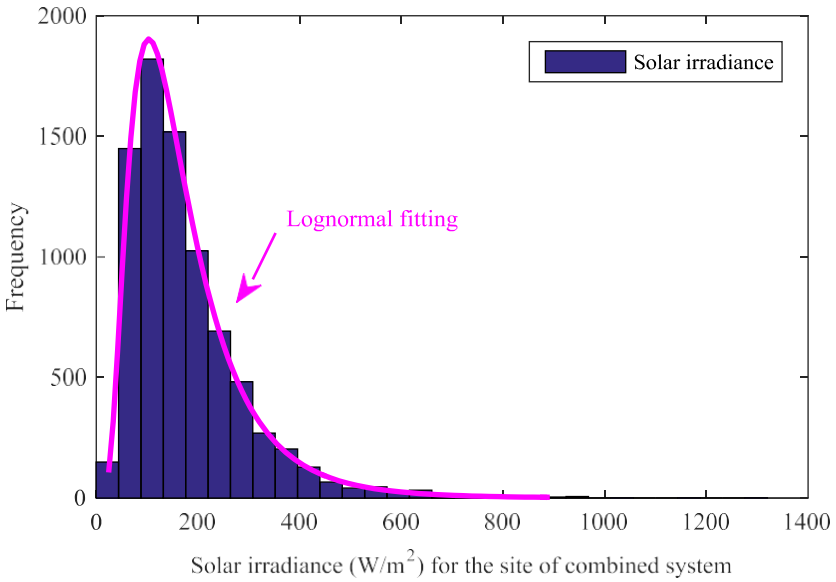

Figure 3.5. Distribution of solar irradiance of the PV plant (8000 samples) regarding bus 13.

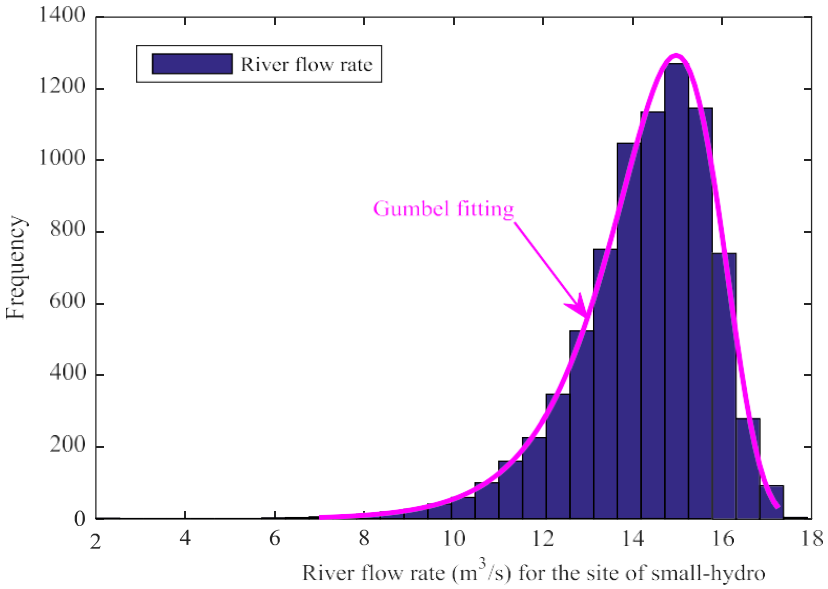

Figure 3.6. Distribution of the flow rate regarding the river for the small hydro plant (8000 samples) at bus 13.

A solar PV unit mixed with a small hydro is attached to bus number 13 of the revised IEEE 30 bus network. Distribution of solar insolation along with lognormal fitting can be detected in Fig. 3.5 while in Fig. 3.6 the flow rate of the river and Gumbel fitting is represented. Both of these figures came out of calculating 8000 Monte-Carlo cases with specified values brought in Table 3.3.

3.7.2 Production Power of PV, Small Hydro and Wind Plants

At bus 5 there are 25 turbines and each of them has a 3 MW capacity, making the capacity of the wind farm 75 MW in total. The output power of the turbines is non-identical due to the different wind speed they face. The output power of the wind plant associated with wind speed can be designated as [35]:

$$p_w(v) = \begin{cases} 0, & for \quad v < v_{in} \ \ and \quad v > v_{out} \\ p_{wr}\left(\dfrac{v - v_{in}}{v_r - v_{in}}\right) & for \quad v_{in} \le v \le v_r \\ p_{wr} & for \quad v_r < v \le v_{out} \end{cases} \tag{3.34}$$

where the evaluated output of a wind plant is p_{wr}. Cut-in speed, cut-off speed, and rated speed of a wind plant are v_{in}, v_r and v_{out}, respectively. Enercon E82-E4 wind turbine has been considered in this case study which has a v_{in} of $3\,m/s$, v_r of $16\,m/s$, and v_{out} of $25\,m/s$.

Energy transformation of the PV in relation with the solar insolation is [35]:

$$P_s(G_s) = \begin{cases} P_{sr}\left(\dfrac{G_s^2}{G_{std} R_c}\right) & for \quad 0 < G_s < R_c \\ P_{sr}\left(\dfrac{G_s}{G_{std}}\right) & for \quad G_s \ge R_c \end{cases} \tag{3.35}$$

where in a normal environment, G_{std} is the solar insolation and set to 1000 W/m^2. Specific insolation point is shown by R_c and set to 120 W/m^2. The evaluated output

power of the solar unit is shown with P_{sr} and all these values are true for both of the PVs connected to buses 11 and 13.

The output power of the small-hydro unit is mathematically calculated as [47]:

$$P_H(Q_h) = \eta \rho g Q_h H_{hyd} \tag{3.36}$$

where Q_h is the flow rate of the water, H_{hyd} is the productive pressure head, the effectiveness of turbine-generator joining is η, the water density is shown with ρ and gravity acceleration is g. These values are set as $H_{hyd} = 25\,m$, $\eta = 0.85$, $\rho = 1000$ kg/m^3 and $g = 9.81\,m/s^2$.

3.7.3 Computation of Probabilities of Wind Power

In zones like beneath the cut-in speed or beyond the cut-off speed, output production of the wind turbine is zero. When the wind speed is in the zone between rated and cut-off speed, the output power of the turbine is p_{wr}. The possibility of wind power output for these separate zones can be calculated as [54]:

$$f_w(p_w)\{p_w = 0\} = 1 - \exp\left[-\left(\frac{v_{in}}{\alpha}\right)^{\beta}\right] + \exp\left[-\left(\frac{v_{out}}{\alpha}\right)^{\beta}\right] \tag{3.37}$$

$$f_w(p_w)\{p_w = p_{wr}\} = \exp\left[-\left(\frac{v_r}{\alpha}\right)^{\beta}\right] - \exp\left[-\left(\frac{v_{out}}{\alpha}\right)^{\beta}\right] \tag{3.38}$$

where wind speed is shown with v, cut-in speed is v_{in}, cut-off speed is v_{out}, and evaluated/rated wind speed is v_r.

When the speed of the wind is in the zone between cut-in and rated speed, wind output power probability which is continuous can be formulated as [33, 35]:

$$f_w(p_w) = \frac{\beta(v_r - v_{in})}{\alpha^{\beta} * p_{wr}} \left[v_{in} + \frac{p_w}{p_{wr}}(v_r - v_{in}) \right]^{\beta-1} \exp\left[-\left(\frac{v_{in} + \frac{p_w}{p_{wr}}(v_r - v_{in})}{\alpha} \right)^{\beta} \right] \quad (3.39)$$

3.7.4 Computing Over and Understimation Price of Production for PV Unit

The accessible power of solar irradiance for the PV plant that is connected to bus number 11 is shown in Fig. 3.7. Achieving all of the accessible solar power may not be possible due to the limited capacity of the PV plant and the accessories of it. Furthermore, the non-public owner of the PV unit may not be eligible to pay the penalty fee above the evaluated capacity of the unit. The actual power of the PV unit that can be carried out is represented in Fig. 3.8. Scheduled power is the quantity that is commonly accepted between the non-public operator and ISO which could be selected from any point of the x-axis of the representation. This scheduled power is illustrated in magenta with a dashed line. The overestimation price in Eq. (3.8) can be achieved with [35]:

$$C_{Rs}(P_{ss} - P_{sav}) = K_{Rs}(P_{ss} - P_{sav}) = K_{Rs} \sum_{n=1}^{N_b^-} [P_{ss} - P_{sn-}] * f_{sn-} \quad (3.40)$$

where the accessible power is shown with P_{sn-} and P_{ss} is the scheduled power. f_{sn-} is the comparative frequency of event of P_{sn-} and the number of PDF duos (P_{sn-}, f_{sn-}) generated is specified with N_b^-. As it can be seen in Fig. 3.8 bigger number of portions (bins) does not significantly make the outcome better. Hence, to be practical, an overall number of 30 bins are chosen for N_b.

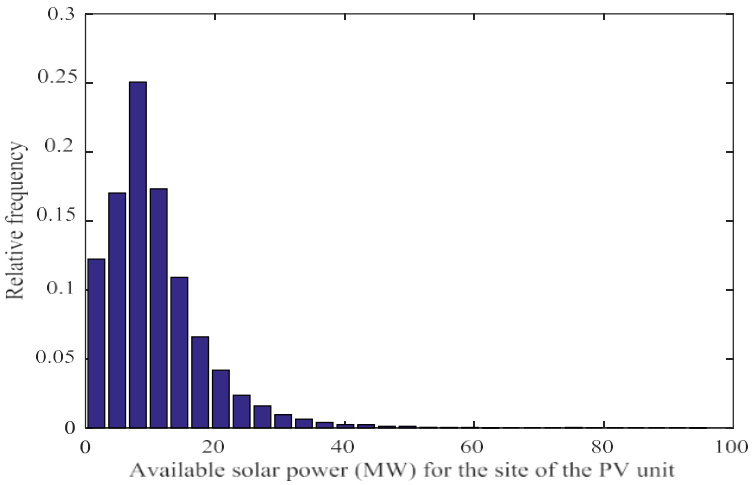

Figure 3.7. Solar irradiance accessible power for the PV plant site at bus number 11.

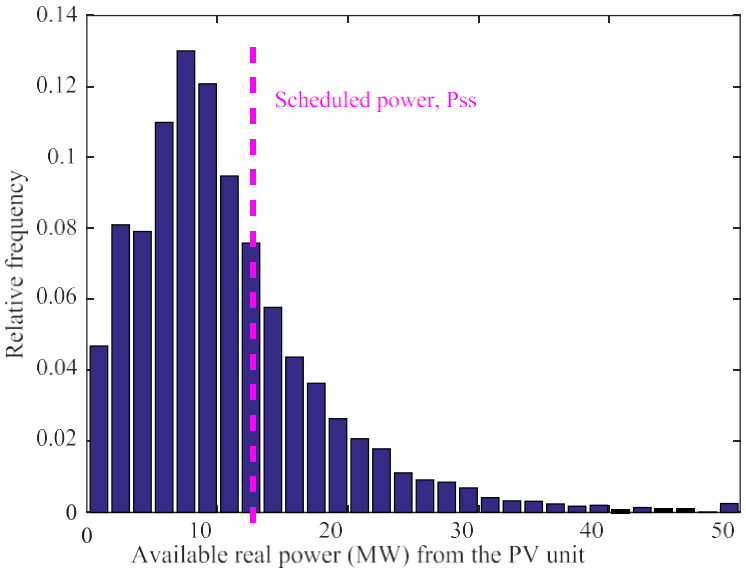

Figure 3.8. Accessible actual power distribution from the PV plant at bus number 11.

ISO must endure a defined penalty price of underestimation for the power of the solar plant. The penalty price stated in Eq. (3.9) is formulated as [35]:

$$C_{Ps}(P_{sav} - P_{ss}) = K_{Ps}(P_{sav} - P_{ss}) = K_{Ps}\sum_{n=1}^{N_b^+}\left[P_{sn+} - P_{ss}\right] * f_{sn+} \tag{3.41}$$

where the accessible power is shown with P_{sn+}. f_{sn+} is the comparative frequency of event of P_{sn+} and the number of PDF duos (P_{sn+}, f_{sn+}) generated is specified with N_b^+.

3.7.5 Computing Over and Underestimation Price of Production for Hybrid Unit

Fig. 3.9 displays accessible solar power for the solar generator site as well as the PV plant attached to bus number 13. The chosen hydro plant connected to bus number 13, have greater evaluated power compared to accessible hydro-power computed from the stochastic flow rate of the river. Accessible hydro production of the site as well as the hydro plant (which are the same) is shown in Fig. 3.10. Output power from the two plants is summed and the combined stochastic output of the power can be seen in Fig 3.11. Elementary calculation of point-by-point summation of 8000 Monte Carlo sets, of two collections of distribution power value (equivalent to the relevant PDFs), is executed to illustrate Fig. 3.11. As previously stated, the small-hydro plant may not be eligible for the penalty or reserve cost. Nevertheless, since the contribution of this unit is trivial compared to the total power shown in Fig. 3.11, the penalty and reserve price are computed by counting the hydro-plant out for ease.

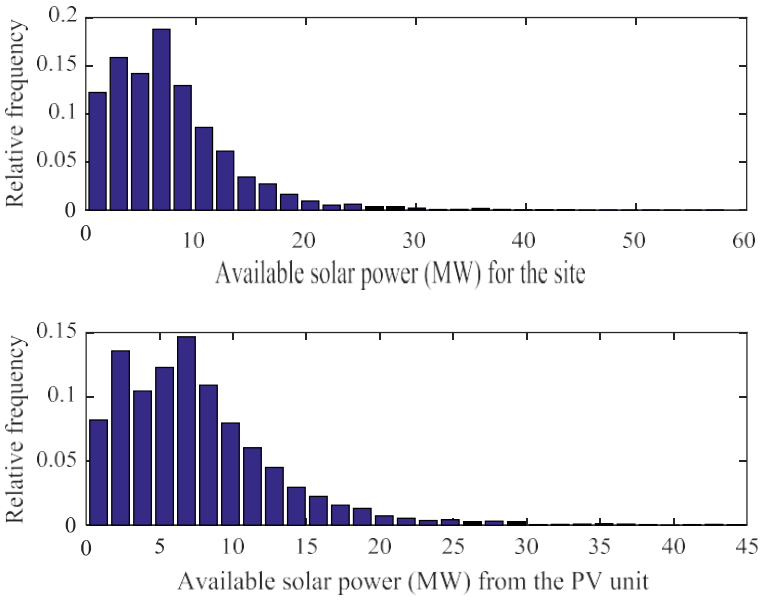

Figure 3.9. Accessible power of solar from the PV plant's site at bus number 13.

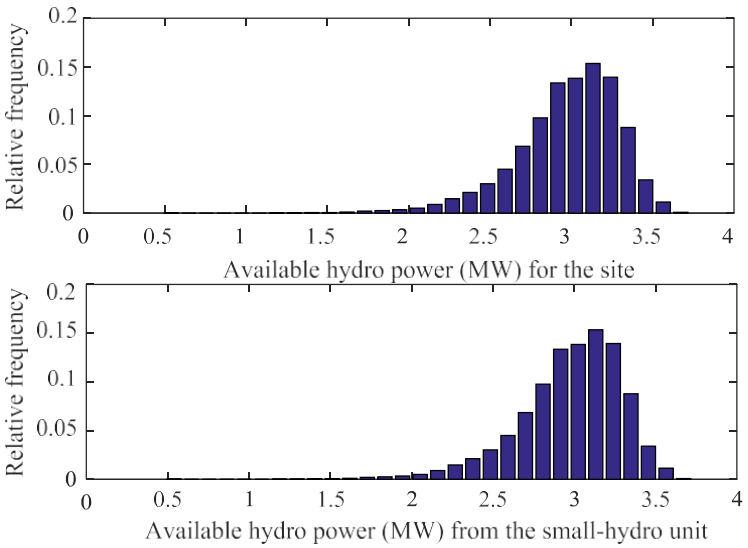

Figure 3.11. Accessible power of hydro from the small hydro plant's site at bus number 13.

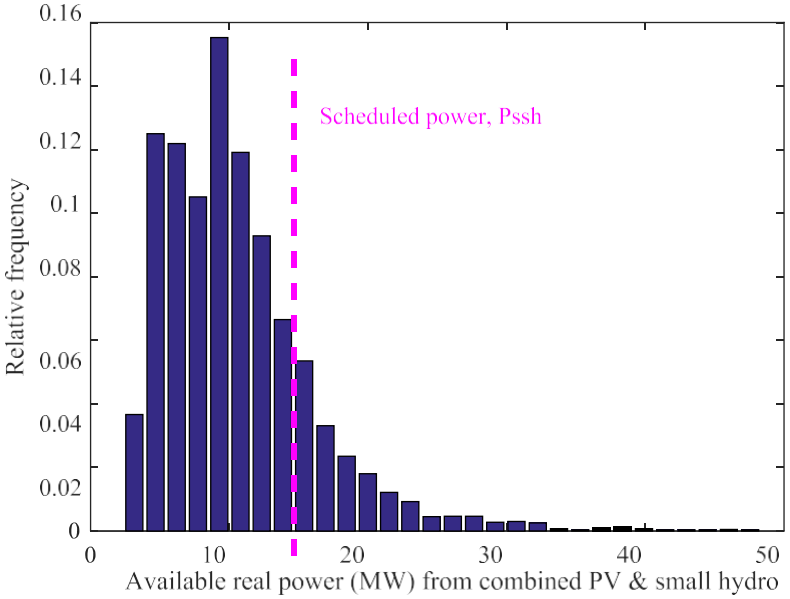

Figure 3.10. All accessible actual power of hybrid unit at bus number 13.

Similar to Eq. (3.40), the overestimation price for the combined network can be shown with [40]:

$$C_{Rsh}(P_{ssh} - P_{shav}) = K_{Rsh}(P_{ssh} - P_{shav}) = K_{Rsh}\sum_{n=1}^{N_b^-}\left[P_{ssh} - P_{shn-}\right] * f_{shn-} \tag{3.42}$$

where the accessible power is shown with P_{shn-} and P_{ssh} is the scheduled power. f_{shn-}

is the comparative frequency of event of P_{shn-} and the number of PDF duos (P_{shn-}, f_{shn-}) generated is specified with N_b^-. Succeeding Eq. (3.41), underestimation price cost of the mixed system can be formulated as [40]:

$$C_{Psh}(P_{shav} - P_{ssh}) = K_{Psh}(P_{shav} - P_{ssh}) = K_{Psh}\sum_{n=1}^{N_b^+}[P_{shn+} - P_{ssh}] * f_{shn+} \tag{3.43}$$

where the accessible power is shown with P_{shn+} and P_{ssh} is the scheduled power. f_{shn+} is the comparative frequency of event of P_{shn+} and the number of PDF duos (P_{shn+}, f_{shn+}) generated is specified with N_b^+.

Table 3.4. Fee ($/MW) coefficients for uncertain source of renewable plants.

Direct coefficient for fees			Reserve coefficient for fees			Penalty coefficient for fees		
Bus 5 For wind	Bus 11 and 13 For solar	Bus 13 For small hydro	Bus 5 For wind	Bus 11 and 13 For solar	Bus 13 For hybrid plant	Bus 5 For wind	Bus 11 and 13 For solar	Bus 13 For hybrid plant
g_w	h_s	m_h	K_{Rw}	K_{Rs}	K_{Rsh}	K_{Pw}	K_{Ps}	K_{Psh}
= 1.7	= 1.6	= 1.5	= 3	= 3	= 3	= 1.4	= 1.4	= 1.4

Table 3.4 [40] shows the evaluated direct price, reserve, and penalty price coefficients of uncertain solar, small hydro, and wind power. As it can be seen, it is decided that the highest direct price coefficient belongs to wind energy and then solar energy and after that, hydro power. The Reserve price coefficient is more than the corresponding direct price coefficient in order to maintain spinning reserve, but the penalty price is less than the direct price for not using the accessible power.

3.8 Multi-Objective Optimization

3.8.1 Constraint Handling Technique (CH)

The first introduction of CH to deal with infeasible solutions is presented in [55]. Later

on, Deb [56] introduced a tolerance parameter to handle constraints by first converting equality constraints into inequality constraints. Modifying tournament selection of the solution is one way to deal with constraints, where initially two random solutions are chosen from the population and the first-rated solution is selected from that two. Hence, there can be three different cases at maximum: Case (1), both solutions are viable. Case (2), one solution is viable and the other one is not, and case (3) which both are infeasible solutions. But here, a slightly different method is used and named as 'constrained domination' [57]. The 'constrained dominate' definition for two solutions x_i and x_j happens when x_i dominate x_j with any of the subsequent rules to be true:

1. Solution x_i is viable whereas x_j is not feasible.
2. Both solutions x_i and x_j are infeasible except x_i has lesser overall boundaries violation and it can be calculated by normalizing all constraint violations and summing them together [57]:

$$CV(x) = \sum_{j=1}^{J} \left\langle \overline{g_j}(x) \right\rangle + \sum_{k=1}^{K} abs\left(\overline{h_k}(x) \right) \tag{3.44}$$

where the expected value $\langle \alpha \rangle$ is $-\alpha$, if $\alpha < 0$, otherwise it is zero. The normalization process can be achieved by:

$$\overline{g_j}(x) = \left(\langle g_j(x) \rangle - \langle g_j \rangle_{\min} \right) / \left(\langle g_j \rangle_{\max} - \langle g_j \rangle_{\min} \right) \tag{3.45}$$

where $\langle g_j \rangle_{\min}$ and $\langle g_j \rangle_{\max}$ are minimum and maximum population constraint violations respectively.

3. Both solutions x_i and x_j are viable and the first solution is superior to the latter by the following rules to be both true:

a) The solution x_i is not inferior to the solution x_j in every aspect.

b) The solution x_i is rigorously superior to the solution x_j in one aspect at least.

3.8.2 Crossover

Crossover is one of the genetic operators that support the blend of the genetic component of two or higher solutions [58]. It can be said that applying crossover is one of the major differentiating characteristics of a genetic algorithm [59]. Some examples of crossover methods for mixing the parent solution and producing offspring (child) are [60]:

1. partially-mapped crossover (PMX)
2. cycle crossover (CX)
3. order crossover operator one (OX)
4. order crossover operator two (OX2)
5. position-based crossover operator (POS)

It is very important to select a suitable crossover method since a specific crossover technique works best for a specific problem, for instance, edge recombination operator (ERO) [61] which was proven to work best for the Traveling Salesman Problems, or the enhanced version of it in [62] which further improved the performance of the mentioned ERO. Thus, in this study, Simulated Binary Crossover (SBX) [63] is used due to the fact that any solution can be created in the initialization phase and during the convergence phase, the focus of the search can be increased. In the SBX, to produce offspring c_1 and c_2 from parents y_1 and y_2, first an accidental value u is constructed in the range between 0 and 1. Secondly, by using a polynomial probability distribution [63], the parameter β_q would be computed as [64]:

$$\beta_q = \begin{cases} (u\alpha)^{\frac{1}{\eta_c+1}} & \text{if } u \le \frac{1}{\alpha} \\ \left(\frac{1}{2-u\alpha}\right)^{\frac{1}{\eta_c+1}} & \text{otherwise} \end{cases} \tag{3.46}$$

where $\alpha = 2 - \beta^{-(\eta_c+1)}$ and β is computed as [64]:

$$\beta = 1 + \frac{2}{y_2 - y_1} \min\left[(y_1 - y_l), (y_u - y_2)\right] \tag{3.47}$$

The range of the parameter y is $[y_l, y_u]$ and distribution index of SBX is shown with η_c which can have any non-negative quantity. Changing η_c to a smaller quantity grants offspring to be created far away from parents while a larger quantity allows it to be created near the parents.

Offspring can be computed as [64]:

$$c_1 = 0.5\left[(y_1 + y_2) - \beta_q |y_2 - y_1|\right] \tag{3.48}$$

$$c_2 = 0.5\left[(y_1 + y_2) + \beta_q |y_2 - y_1|\right] \tag{3.49}$$

where $y_1 < y_2$ but modification can be made for $y_1 > y_2$.

3.8.3 Mutation

After crossover, the next protagonist in GA is the mutation operator [58]. Since mutation operator disturbs the solutions based on accidental changes, choosing the correct method is crucial. Constraints narrow the entire solution space into a feasible subspace. Hence, it is sometimes difficult to reach all points inside the solution space and because of that, a correct technique can lead to finding the optimum but an improper one can give bias advantage [58]. Not all mutation operators can ensure the action of finding the global optimum. In fact, some of them work best for one specific problem while for other problems they are not promising. Some known mutation

operators are:

1. displacement mutation operator (DM) [65]
2. exchange mutation operator (EM) [65]
3. scramble mutation operator (SM) [65]
4. inversion mutation operator (IVM) [65]
5. insertion mutation operator (ISM) [65]

In this study, a parameter-based mutation known as polynomial mutation [63] is used. Fig. 3.12 shows a sample code of this operator. The procedure is as follow:

Every control variable has a probability pm to be disrupted. A random number t between 1 and the value of control variables (V) is calculated for every decision variable. If $t < pm$ then the following procedure is applied in order to mutate the variables.

First, a random number u is created in the range between 0 and 1, and the parameter δ_q is calculated as [64]:

$$\delta_q = \begin{cases} \left[2u + (1-2u)(1-\delta)^{\eta_m+1}\right]^{\frac{1}{\eta_m+1}} - 1 & \text{if } u \le 0.5 \\ 1 - \left[2(1-u) + 2(u-0.5)(1-\delta)^{\eta_m+1}\right]^{\frac{1}{\eta_m+1}} & \text{otherwise} \end{cases} \tag{3.50}$$

where the distribution index of mutation is shown with η_m and can have any non-negative quantity. A larger quantity of η_m gives a stronger possibility of establishing offspring within the neighborhood of the parent and a tiny value allows a further solution to be established. For $y \in [y_l, y_u]$ the parameter δ is formulated as [64]:

$$\delta = \min\left[(y - y_l), (y_u - y)\right] / (y_u - y_l) \tag{3.51}$$

where y is the parent solution and the mutated offspring is computed as [64]:

$$c = y + \delta_q \left(y_u - y_l \right) \tag{3.52}$$

Mutation probability (pm) for this study is considered to be $1/V$ where V is the number of decision variables, 11 in this study.

```
real_mutation(value)
float value;
{
float delta, u;
if flip (p_mutation) {
u = random(); /* a random number in (0,1) */
if (u < 0.5)
delta = pow(2*u, (1.0/(n+1))) - 1.0;
else delta = 1.0 - pow(2*(1.0-u), (1.0/(n+1)));
}
else delta = 0.0; /* no mutation */
return (value + delta * Max_mut);
}
```

Figure 3.12. Pseudo code of mutation using polynomial probability distribution [66].

3.8.4 Real Coded NSGA-II

In 1995, a non-dominated sorting genetic algorithm (NSGA) was presented by Srinivas and Deb [67] in order to solve problems of multi-objective optimization. The idea is based on a suggestion given by Goldberg in 1989 [68] and follows even an earlier application of GA introduced in 1984 by Schaffer [69] known as the VEGA algorithm, which opened new doors in the field of multi-objective optimization. Although this algorithm, VEGA, gave promising results at first, but later on it encountered bias approaching some of the *pareto* optimal solutions. Like VEGA, NSGA had some of

its own problems over the years, such as the excessive computational difficulty of non-dominated sorting, absence of elitism, and necessity of defining a sharing parameter. Deb, later on, enhanced his NSGA algorithm to address the above-mentioned issues, the one that is now called NSGA-II or Elitist Non-dominated Sorting Genetic Algorithm. In NSGA-II, there are three characteristics:

1. Elitist concept is used in the algorithm.
2. The algorithm uses a clear technique to preserve diversity.
3. Non-dominated solutions are shown in highlighted by the algorithm.

Each concept will be summarized. Detailed descriptions and definitions are provided in [70].

3.8.5 Quick Non-dominated Sorting Procedure

To determine if the answers of the first non-dominated front are dominated by one another, the simplest way is to compare all of the solutions with each other one by one. Completing this procedure for the first non-dominated front would result in the overall complexity of $O(MN^2)$ where O is the 'Bachmann–Landau' notation (big O notation), M is the value of objectives, and N is the population magnitude. Finding individuals in the second non-dominated level can be achieved by repeating the same procedure only without considering the answers of the first non-dominated front. Again, the same complexity of $O(MN^2)$ is needed and this fact is true for the third and fourth and all other non-dominated levels. Thus, a total complexity of $O(MN^3)$ is necessary for the worst-case scenario in which there exists only a single solution in each level, for N number of fronts.

Fig. 3.13 shows a quicker method with the overall complexity of $O(MN^2)$. n_p means how many times the solution p is dominated, and S_p is a group of solutions dominated

by p. It is worth mentioning that, even though the simplest approach has higher overall complexity, it only requires $O(MN)$ storage whereas the quicker approach has less complexity but it requires $O(MN^2)$ storage.

For the quicker approach, in the first non-dominated front, n_p for all of the solutions are set to zero. Next, for all those solutions with n_p as zero, every representative q of its set S_p is inspected, and its domination magnitude is shortened by one. Afterward, any member q reaching the domination count of zero is placed into another category Q and form the second non-dominated front. Now, the above-mentioned technique is practiced to the members of Q in order to form the third non-dominated front and this operation goes on till every front is established. To compute the complexity of this method, in the first inner loop of Fig. 3.13 (for each $p \in F_i$), since each entity can be part of a maximum of one front, the loop is performed N times exactly. As for the second inner loop (for each $q \in S_p$), each entity can dominate other members $N-1$ time at most, and checking dominated individuals needs no more than M comparisons. Hence, the total complexity of $O(MN^2)$ [70].

```
for each p ∈ P
    S_p = ∅
    n_p = 0
    for each q ∈ P
        if (p≺q) then
            S_p = S_p ∪ {q}
        else if (q≺p) then
            n_p = n_p + 1
     if n_p =0 then
        p_rank = 1
        F_1 = F_1 ∪ {p}
i = 1
while F_i ≠ ∅
    Q_i ≠ ∅
    for each p ∈ F_i
        for each q ∈ S_p
        n_q = n_q − 1
        if n_q =0 then
            q_rank = i + 1
            Q = Q ∪ {q}
  i = i + 1
  F_i = Q
```

Figure 3.13. Pseudo-code for a quicker approach of non-dominated sorting.

3.8.6 Main Loop of NSGA-II

Firstly, an accidental parent population is generated which is called P_0. Population sorting is built on non-domination. Every answer is given a rank corresponding to its non-domination position where rank 1 is the finest level, the best one afterward is rank 2, and the best one after that is rank 3, and it continues. Hence, minimizing the rank is expected. By using normal genetic operators like binary tournament selection, recombining, and mutating, the offspring Q_0 with a population of N is created. At this point, elitism is ready to be applied but first, a description of the t^{th} generation is necessary. The sample code of the t^{th} generation is shown in Fig. 3.16. By combining P_t and Q_t, a new population of size $2N$ is generated which is shown with R_t. Then, non-dominated sorting is enforced by blending the population with points of non-dominated fronts. Filling the population begins with selecting the points from the non-dominated front that has the highest rank (level 1 or F_1) and it continues with selecting

the points of the non-dominated front with the second-best rank (level 2 or F_2) and so on. Because the capacity of R_t is limited to $2N$, there will be some fronts remained. The remaining fronts that cannot be accommodated in, are removed. There also may be a situation when selecting points of the last front like F_3 in Fig. 3.14, which are more than the needed slots for the new population. In this case, the points that add more diversity to the population are chosen. Here is one of the differences between NSGA-II and NSGA, where in the latter, a sharing parameter like δ is required for niching during the tournament selection and population reduction stage whereas in the former, a new method recognized as 'crowding distance' is represented. To calculate the diversity factor, a 'crowding distance' function is used. d_i is called the crowding distance of point i and it is calculated by computing the objective space around the point i that is not inhabited with any other solution. d_i can be acquired by obtaining the cuboid's perimeter shown in Fig. 3.15. This cuboid is made with the assist of the closest neighbors of the point i. Now that the crowding distance is established, the points with the highest crowding distance value are selected for the new population until there is no slot left to fill and the remaining points are removed. Finally, the new population of P_{t+1} with the size of N is formed. In the next step, this population P_{t+1} is used to select, recombine and mutate for generating a new population Q_{t+1} with the size of N.

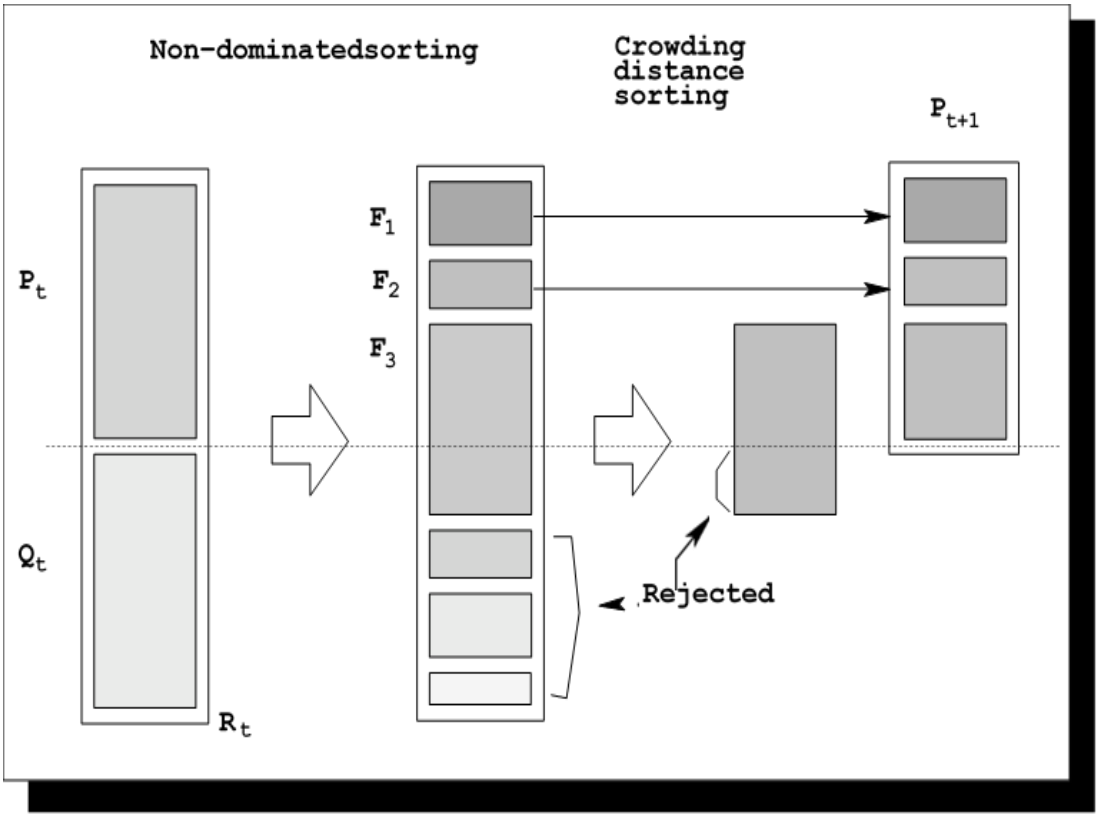

Figure 3.14. Illustration of the mechanism of NSGA-II.

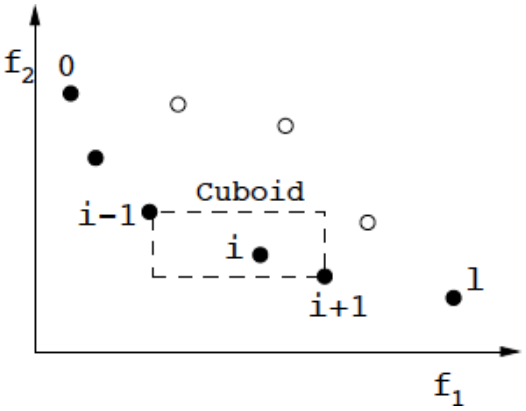

Figure 3.15. The crowding distance calculation.

The illustration in Figure 3.15 is showing how this new crowding distance function brings a new feature for selecting the fronts to be well diverse as the algorithm selects different solutions during the iteration.

$R_t = P_t \cup Q_t$

$F =$ fast non-dominated sort (R_t)

$P_{t+1} = \varnothing$ and $i = 1$

until $\left|P_{t+1}\right| + \left|F_i\right| \le N$

crowding distance assignment (F_i)

$P_{t+1} = P_{t+1} \cup F_i$

$i = i + 1$

Sort(F_i, crowded comparison)

$P_{t+1} = P_{t+1} \cup F_i \left[1 : \left(N - \left|P_{t+1}\right|\right)\right]$

$Q_{t+1} =$ make new population (P_{t+1})

$t = t + 1$

Figure 3.16. Pseudo code of the t^{th} generation.

In Figure 3.17 flowchart of how the algorithm works, is represented. While having multiple objective functions along with constraints, the first step is to find trade-off solutions, meaning that one solution may not be absolutely better than the other one. In the second step, a single solution based on a method of choice like fuzzy decision making [23, 28], same as in this study, will be extracted.

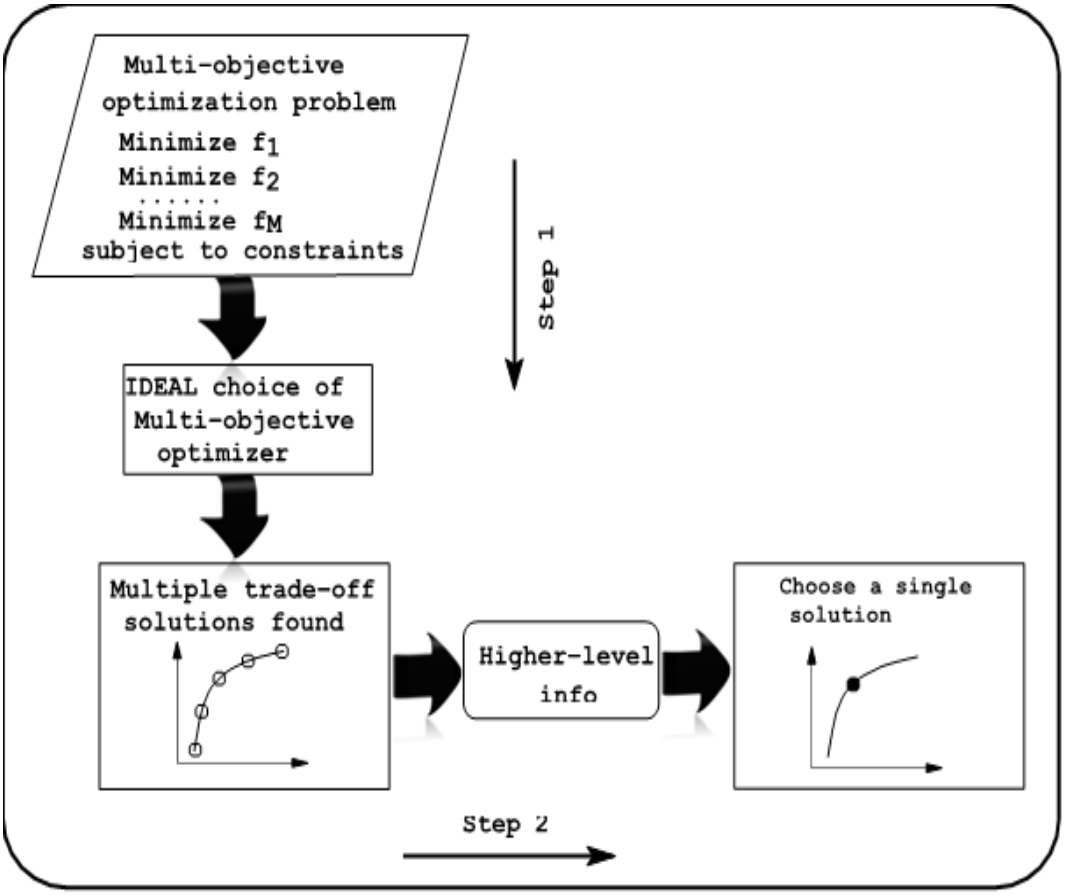

Figure 3.17. Illustration of a two-step multi-objective optimization mechanism.

Chapter 4

SIMULATION RESULTS

Throughout this chapter, the outcome of the simulation practicing real coded NSGA-II algorithms on the altered IEEE 30 bus case is examined and briefed. The algorithm is described in chapter 3. The parameters used for the method are listed in Table 4.1.

Table 4.1. Defined parameters for real coded NSGA-II.

R-NSGA-II	
Parameter	Value
Size of the population	200
Maximum iteration amount	650
Distribution index of crossover, η_c	20
Distribution index for mutation, η_m	100
Number of decision variables, V	11
Number of runs	21
Mutation probability, pm	1/11

4.1 Simulation Results of the Algorithms

Comprehensive results of the simulations along with settings of decision variables are presented in Table 4.2. Also, the results of this simulation are compared with two other algorithms shown in Table 4.3 to ensure the effectiveness of the developed method.

A single best objective for both emission and cost is selected, out of all runs of the simulation which gives the minimum value for the specified objective. Decision variables are:

1. The actual power of the generator (excluding slack unit, P_{TG1})
2. Generator bus voltages from scheduled production of solar, wind and hybrid

(mixed solar and hydro) plants (P_{ws}, P_{ss}, and P_{ssh} respectively)

POZs are introduced for thermal generator $TG2$ to add discontinuity. The range of the POZ is provided in Table 4.2. The real power of P_{TG1} and the imaginary power of all generators are variables that are considered as restrictions and should be satisfied by the algorithm. Accumulated voltage drops of load buses (VD) is also provided. The contribution of the small-hydro plant is shown with $P_{ssh,h}$.

Table 4.2. Simulation results of the real coded R-NSGA-II optimization algorithms.

Control & state variables	Min	Max	real coded NSGA-II – Best solutions		
			Cost	Emission	Comp
P_{TG1} (MW)	50	140	139.365	50.031	113.435
P_{TG2} (MW)	20	80	54.066	48.861	65
POZ (for $TG2$): from [30,40] and [55,65]					
P_{TG3} (MW)	10	35	11.206	34.455	20.525
P_{ws} (MW)	0	75	52.209	74.704	54.530
P_{ss} (MW)	0	50	17.639	49.198	18.964
P_{ssh} (MW)	0	50	15.445	28.572	16.444
V_1 ($p.u.$)	0.95	1.10	1.0790	1.0671	1.0832
V_2 ($p.u.$)	0.95	1.10	1.0645	1.0598	1.0691
V_5 ($p.u.$)	0.95	1.10	1.0423	1.0454	1.0485
V_8 ($p.u.$)	0.95	1.10	1.0397	1.0386	1.0367
V_{11} ($p.u.$)	0.95	1.10	1.0877	1.0729	1.0350
V_{13} ($p.u.$)	0.95	1.10	1.0608	1.0274	1.0386
Q_{TG1} ($MVAr$)	-50	140	3.7384	10.021	13.474
Q_{TG2} ($MVAr$)	-20	60	21.473	21.707	24.726
Q_{TG3} ($MVAr$)	-15	40	39.771	33.554	38.055
Q_{ws} ($MVAr$)	-30	35	26.316	25.922	31.426
Q_{ss} ($MVAr$)	-20	25	24.997	24.436	9.3649
Q_{ssh} ($MVAr$)	-20	25	20.570	10.359	15.708
Total fee ($\$/h$)			**892.760**	1017.4	**924.864**
Emission (t/h)			2.3231	**0.0959**	**0.5111**
VD ($p.u.$)			0.4524	0.4507	0.4753
$P_{ssh,h}$ (MW)			3.2648	3.0753	3.1518

In Table 4.5 the best cost and the best emission is picked up from the 21 runs of the

simulation. A detailed explanation is provided in the upcoming paragraphs regarding the best comp solution.

In the next tables, the results of the R-NSGA-II with two other algorithms will be compared in different cases to show the robustness of the developed algorithm.

4.1.1 Provisional Study of the Results and Comparison

In Table 4.3 results of two previously used methods along with the proposed method are provided. SMODE-SF, as well as MOEA/D-SF, are both done in Ref. [40] with the same configuration.

Table 4.3. Comparison between R-NSGA-II and two previous algorithms in case of best pareto front (highest hypervolume indicator).

Decision variables	MOEA/D-SF		SMODE-SF		R-NSGA-II	
	Best cost	Best emission	Best cost	Best emission	Best cost	Best emission
P_{TG1} (MW)	139.297	62.280	139.112	50.072	139.731	50.005
P_{TG2} (MW)	55	70.051	55	52.627	55	52.228
P_{TG3} (MW)	10.622	35	10	34.919	10.490	34.823
P_{ws} (MW)	52.380	68.682	53.714	71.168	52.227	74.917
P_{ss} (MW)	17.348	31.034	16.167	29.555	17.614	49.686
P_{ssh} (MW)	15.328	19.509	16.057	48.254	14.965	24.513
V_1 ($p.u.$)	1.0806	1.0690	1.0825	1.0732	1.0813	1.0805
V_2 ($p.u.$)	1.0659	1.0653	1.0646	1.0572	1.0693	1.0689
V_5 ($p.u.$)	1.0384	1.0473	1.0387	1.0076	1.0459	1.0448
V_8 ($p.u.$)	1.0376	1.0420	1.0316	1.0302	1.0375	1.0370
V_{11} ($p.u.$)	1.0866	1.0681	1.0696	1.0691	1.0771	1.0046
V_{13} ($p.u.$)	1.0615	1.0582	1.0633	1.0160	1.0423	1.0271
Q_{TG1} ($MVAr$)	5.317	-0.89	13.849	32.209	0.8551	24.718
Q_{TG2} ($MVAr$)	26.047	27.845	21.72	29.609	33.465	29.655
Q_{TG3} ($MVAr$)	37.51	34.543	32.692	36.783	37.359	34.835
Q_{ws} ($MVAr$)	22.139	25.022	24.920	-5.19	28.204	21.447
Q_{ss} ($MVAr$)	24.903	18.508	20.113	24.951	22.563	3.1901
Q_{ssh} ($MVAr$)	21.131	20.416	23.70	8.624	14.565	13.571
Total fee ($\$/h$)	893.003	989.276	893.503	1018.786	**892.933**	1016.371
Emission (t/h)	2.3134	0.1091	2.2868	**0.0961**	2.3774	**0.0961**
VD ($p.u.$)	0.4464	0.4382	0.4304	0.5388	0.4305	0.5827
$P_{ssh,h}$ (MW)	3.50	3.20	3.131	3.254	3.2839	3.1603

Results of Table 4.3 are abducted from the best *pareto* front of the best run among all 21 runs. Then, the ones with the lowest cost and emission are selected separately, to be represented in the table as the best results for the respected objective.

4.1.2 Best Compromised Solution

The method of calculating the best *pareto* front is a delicate formula. As mentioned before, there is no absolute best solution when comparing results of multi-objective optimization. One algorithm can provide results for the best cost or emission on a single side of view, and it is easy to choose the best cost as an output target or the best emission for that matter, among all the available outcomes. But when it comes to considering both cost and emission together, for instance, making cost better will result in making emission worse or vice versa. To overcome that, two steps can be done while making the decision of choosing the best result.

The first step is to choose the best result among all the results of the trial runs. In order to do that, a method known as hypervolume indicator [71, 72] is used to determine which one of the *pareto* fronts is the best one. Now, after this step, the best cost or the best emission can be chosen for comparison, like in Table 4.3. It can be seen from the results that R-NSGA-II has the best cost among all the algorithms. As for the emission, it outperforms the MOEA/D-SF and gives the same emission value as SMODE-SF. It is fair to say that in overall comparison, R-NSGA-II is superior to the other two algorithms. A detailed explanation of the superiority will be given further in this chapter.

4.1.3 Fuzzy Decision Making

The second step is to designate the best-compromised solution out of the best *pareto* front. For that, famous fuzzy decision-making has been applied to obtain the best-compromised solution out of all answers in the best *pareto* front. The reason for that

name as mentioned is because while trying to make cost or emission better, the other objective would become worse in the process, hence compromising is needed. Comparing the compromised solution with each other may not make sense since none of the algorithms will give the best emission and cost at the same time in this case. Computing fuzzy decision making can be formulated as [40]:

$$\xi_m^k = \begin{cases} 1 & for \quad f_m^k \le f_m^{\min} \\ \dfrac{f_m^{\min} - f_m^k}{f_m^{\max} - f_m^{\min}} & for \quad f_m^{\min} < f_m^k < f_m^{\max} \\ 0 & for \quad f_m^k \ge f_m^{\max} \end{cases} \tag{4.1}$$

Where ξ_m^k defines the value of membership function for m^{th} the objective of k^{th} the non-dominated solution. M^{th} objective fitness value for k^{th} the non-dominated solution is shown with f_m^k, maximum fitness number of the *m*-th objective function between all of the non-dominated answers is designated with $f_m^{\max}$ and minimum fitness value of the same function is represented with $f_m^{\min}$.

4.1.4 Hypervolume Indicator

In a naive definition, the hypervolume indicator will consider the amount of area that is accumulated under or above a pretor front set while considering a set of reference points that is going to be needed for comparison. To make it simplified it can be said that the bigger the area is, the better the indicator becomes. Thus, the biggest output of the hypervolume indicator is chosen according to a set of reference points which are [1,1] in this study.

Table 4.4 shows a comparison between hypervolume indicator results from the algorithm in this study as well as two more algorithms from a previous study [40]. Min, max, mean along with the standard deviation of the hypervolume indicator are

displayed and compared and R-NSGA-II has the highest hypervolume indicator with an acceptable standard deviation among them.

Table 4.4. Comparison of HV numbers of algorithms.

Algorithm	Maximum	Minimum	Mean	Std Deviation
MOEA/D-SF	0.8352	0.8337	0.8346	0.0004
SMODE-SF	0.8707	0.8635	0.8684	0.0026
R-NSGA-II	0.8842	0.8577	0.8679	0.0071

Table 4.5 represents the comparison between the discussed algorithm, solely based on their single objective value which is picked from one of the 21 runs of the simulation and it gives the best value for the cost and emission. The best-compromised solution was first picked from the run having the highest hypervolume indicator value and then extracted via the fuzzy decision-making method.

4.2 Detailed Analysis

To understand more about the superiority of the R-NSGA-II algorithm compared to the other two above-mentioned algorithms, analysis and explanation are provided in the next paragraphs.

4.2.1 Superiority of the Proposed Method

Comparing the total annual fees of the network is one of the ways of showing robustness since the central objective of economic dispatch is to bring down the price. For that purpose, from Table 4.3, R-NSGA-II can save $595.68 in a year compared to MOEA/D-SF and it can save $4,975.68 yearly compared to SMODE-SF. These results are in the case that, best *pareto* front (highest hypervolume indicator) is selected. In the case that only the best individual cost is selected (out of 21 runs), from Table 4.5, the R-NSGA-II method provides $1,795.8 less cost compared to the MOEA/D-SF method in a year, and it can save $4,853.04 each year when comparing it to the SMODE-SF algorithm and it gives less emission at the same time meaning that R-

NSGA-II completely dominates SMODE-SF method in multi-objective comparison of cost and emission. R-NSGA-II outperforms MOEA/D-SF as well in a single objective comparison of emission and cost separately, meaning that comparing the best section of cost and the best section of emission yields the superiority of the R-NSGA-II method. Thus, R-NSGA-II is superior to both the other algorithms above.

It is worth mentioning that the results across all 21 runs of the simulation are found to be consistent, meaning that the superiority of R-NSGA-II did not randomly happen in a single case but in all cases (Table 4.7).

Table 4.6 illustrates the worst *pareto* front (lowest hypervolume indicator) among all 21 runs. Comparing these results with the results of Table 4.3 (best *pareto* front of MOEDA/D-SF and SMODE-SF in this case), it can be observed that the R-NSGA-II method totally dominates the MOEA/D-SF algorithm in the *best cost* section, meaning that the value of total cost ($/h) and emission (t/h) provided by R-NSGA-II are lower and also in the *best emission* section, the value of emission (t/h) provided by R-NSGA-II is lower as well. Also, when comparing the worst *pareto* front of R-NSGA-II with the best *pareto* front of SMODE-SF, in the *best cost* section R-NSGA-II is superior and in the *best emission* section, R-NSGA-II is not far behind.

Table 4.5. Comparison between R-NSGA-II and two previous methods in the case of best objectives.

Decision parameters	Min	Max	MOEA/D-SF			SMODE-SF			real coded NSGA-II		
			Best comp	Best cost	Best emission	Best comp	Best cost	Best emission	Best comp	Best cost	Best emission
P_{TG1} (MW)	50	140	117.118	139.048	60.003	111.91	139.848	50.047	113.435	139.365	50.031
P_{TG2} (MW)	20	80	65	53.763	65	65	55	47.535	65	54.066	48.861
P_{TG3} (MW)	10	35	18.403	11.558	34.890	23.555	10	35	20.525	11.206	34.455
P_{ws} (MW)	0	75	55.447	52.616	74.290	54.058	53.391	74.282	54.530	52.209	74.704
P_{ss} (MW)	0	50	17.649	17.593	28.529	18.436	16.818	50	18.964	17.639	49.198
P_{ssh} (MW)	0	50	15.326	15.319	23.755	15.755	14.989	29.336	16.444	15.445	28.572
V_1 ($p.u.$)	0.95	1.10	1.076	1.0785	1.0545	1.0761	1.0823	1.0738	1.0832	1.0790	1.0671
V_2 ($p.u.$)	0.95	1.10	1.0648	1.0644	1.0465	1.0662	1.0672	1.0596	1.0691	1.0645	1.0598
V_5 ($p.u.$)	0.95	1.10	1.0444	1.0436	1.0277	1.0362	1.0406	1.0393	1.0485	1.0423	1.0454
V_8 ($p.u.$)	0.95	1.10	1.0402	1.0398	1.0232	1.0362	1.0345	1.0196	1.0367	1.0397	1.0386
V_{11} ($p.u.$)	0.95	1.10	1.0878	1.0876	1.0619	1.0778	1.0743	1.0576	1.0350	1.0877	1.0729
V_{13} ($p.u.$)	0.95	1.10	1.0602	1.0622	1.0457	1.0432	1.0668	1.0481	1.0386	1.0608	1.0274
Q_{TG1} ($MVAr$)	—50	140	2.128	2.736	8.771	2.788	7.191	28.944	13.474	3.7384	10.021
Q_{TG2} ($MVAr$)	—20	60	21.410	21.153	19.405	34.504	27.547	21.749	24.726	21.473	21.707
Q_{TG3} ($MVAr$)	—15	40	37.727	39.396	31.835	36.169	33.207	9.100	38.055	39.771	33.554
Q_{ws} ($MVAr$)	—30	35	27.102	27.549	22.165	20.376	24.238	25.342	31.426	26.316	25.922
Q_{ss} ($MVAr$)	—20	25	24.911	24.836	22.017	23.410	20.801	21.241	9.3649	24.997	24.436
Q_{ssh} ($MVAr$)	—20	25	20.328	21.071	21.514	15.620	24.052	20.950	15.708	20.570	10.359
Total fee ($\$/h$)			919.040	892.954	994.342	927.049	893.314	1020.490	924.864	**892.760**	1017.4
Emission (t/h)			0.6221	2.2772	0.1052	0.4721	2.3950	**0.0959**	0.5111	2.3231	**0.0959**
VD ($p.u.$)			0.4530	0.4567	0.4542	0.4215	0.4369	0.468	0.4753	0.4524	0.4507
$P_{ssh,h}$ (MW)			3.50	3.50	3.135	3.296	3.163	3.183	3.1518	3.2648	3.0753

Table 4.6. Worst pareto front (lowest hypervolume indicator) of the R-NSGA-II.

Control variables	Min	Max	Cost	Emission	Comp
P_{TG1} (MW)	50	140	139.201	50.008	114.154
P_{TG2} (MW)	20	80	54.236	65	65
P_{TG3} (MW)	10	35	11.254	34.881	20.911
P_{ws} (MW)	0	75	52.220	74.231	55.205
P_{ss} (MW)	0	50	17.575	29.350	17.935
P_{ssh} (MW)	0	50	15.441	32.629	15.580
V_1 ($p.u.$)	0.95	1.10	1.0801	1.0657	1.0760
V_2 ($p.u.$)	0.95	1.10	1.0651	1.0615	1.0659
V_5 ($p.u.$)	0.95	1.10	1.0423	1.0476	1.0420
V_8 ($p.u.$)	0.95	1.10	1.0394	1.0411	1.0393
V_{11} ($p.u.$)	0.95	1.10	1.0866	1.0834	1.0817
V_{13} ($p.u.$)	0.95	1.10	1.0551	1.0663	1.0624
Q_{TG1} ($MVAr$)	-50	140	5.5975	1.5613	0.9469
Q_{TG2} ($MVAr$)	-20	60	21.707	19.965	26.886
Q_{TG3} ($MVAr$)	-15	40	39.755	30.905	36.273
Q_{ws} ($MVAr$)	-30	35	26.188	25.549	24.388
Q_{ss} ($MVAr$)	-20	25	24.990	23.353	22.870
Q_{ssh} ($MVAr$)	-20	25	18.600	22.310	21.581
Total fee ($\$/h$)			**892.767**	1006.8	**923.28**
Emission (t/h)			2.2993	0.0983	**0.5030**
VD ($p.u.$)			0.4387	0.4784	0.4469
$P_{ssh,h}$ (MW)			3.3403	2.9464	2.9494

In Table 4.7 only the best cost of all 21 runs is provided. It can be seen that the lowest cost among the trial runs of the proposed algorithm is from run number 5, with the value of 892.7606($/h) and the highest cost result calculated by the R-NSGA-II algorithm is from trial run number 11 with a value of 892.9335($/h), which interestingly has the highest hypervolume indicator among all runs. This means that in the worst-case scenario, the results provided by the proposed R-NSGA-II algorithm is better than the results provided by the other two algorithms in their best-case scenarios. Hence, the significance of the results and strength of the proposed algorithm are seen.

Furthermore, the consistency of the results is visible in Table 4.7 and the standard deviation of the whole set is 0.0400 which again adds more clarity to the results being consistent.

Table 4.7. Results of the cost of the real coded R-NSGA-II optimization algorithm in all 21 runs of the simulation.

Run	Cost ($/h)
1	892.7732
2	892.7820
3	892.7993
4	892.7728
5	892.7606
6	892.8236
7	892.7960
8	892.7701
9	892.7789
10	892.7790
11	892.9335
12	892.7886
13	892.7919
14	892.8735
15	892.7777
16	892.7877
17	892.7910
18	892.7631
19	892.7889
20	892.7670
21	892.7843

4.2.2 Configuration and Characteristic of the Algorithm

Figure 4.1 displays the range of solutions provided by the R-NSGA-II method and it is obtained from the best individual cases of cost and emission throughout the 21 runs. Figure 4.2 compares the best as well as worst *pareto* front (highest and lowest hypervolume indicator) of the same method. The algorithm is well diverse and the difference between the worst and best *pareto* fronts is trivial and in terms of convergence, the difference is negligible as well. The average time of calculation is 387.38 seconds for each trial. The R-NSGA-II algorithm is developed/coded using MATLAB and simulations are executed on a PC with Intel Core i3 10th generation

CPU @3.5 GHz with 8GB of RAM.

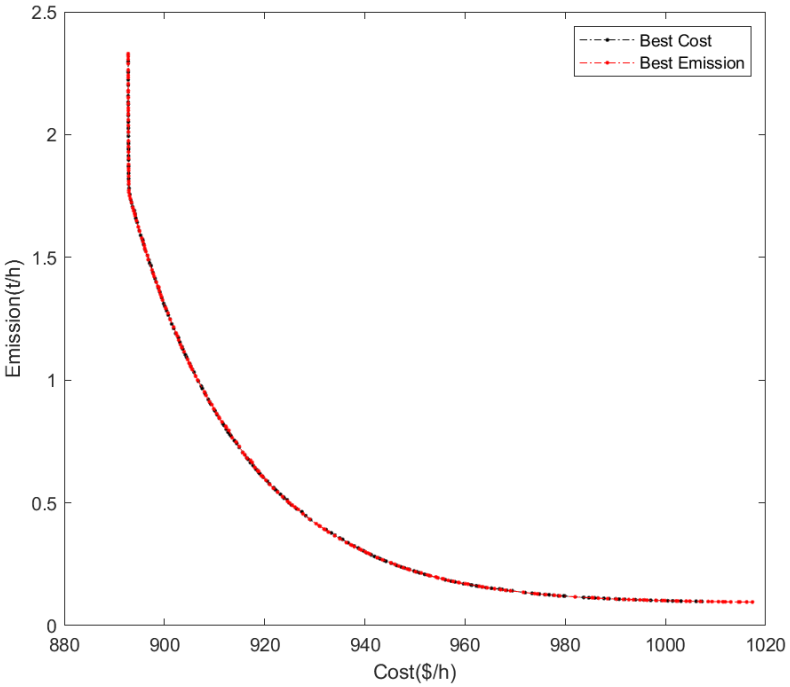

Figure 4.1. Pareto fronts of R-NSGA-II method in best and worst cases.

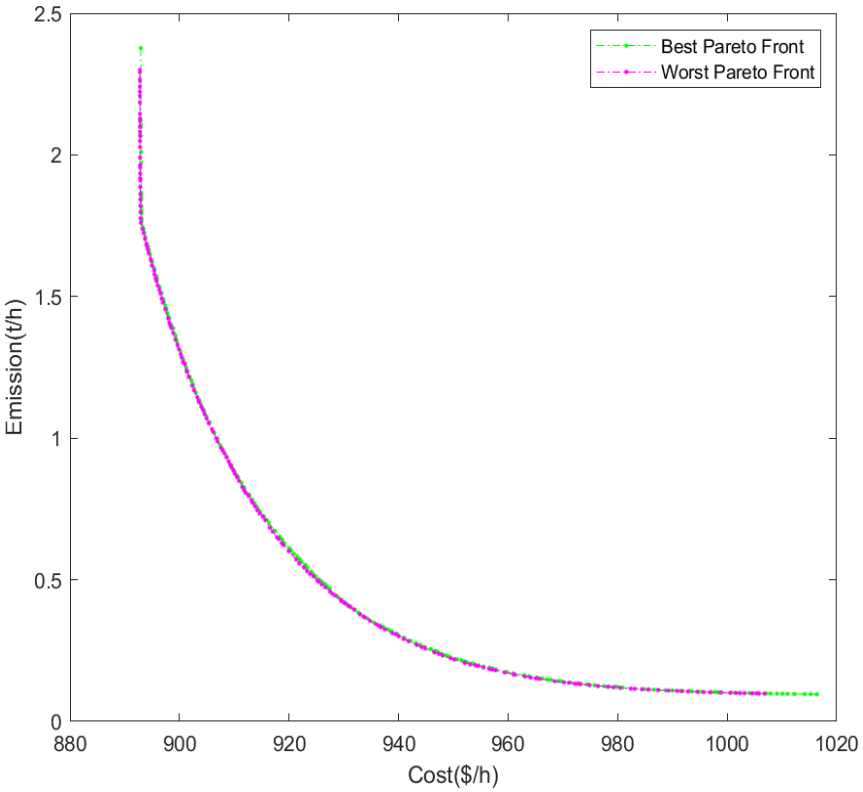

Figure 4.2. Best cost and emission of R-NSGA-II method.

4.2.3 Critical Analysis

The worst (highest) Voltage Drop (VD) value provided by MOEA/D-SF among all 21 runs is reported to be 0.5704 p. u. and the same value for SMODE-SF is reported to be 0.6201 p. u. while the worst VD value provided by R-NSGA-II is 0.4607 p. u. and Fig 4.3 display all VD values for 21 runs of the simulation.

The consistency of the VD values is shown in Fig 4.3 with having 0.4165 as the minimum (the best) VD and 0.4607 being the maximum value (the worst) with a standard deviation of 0.0119.

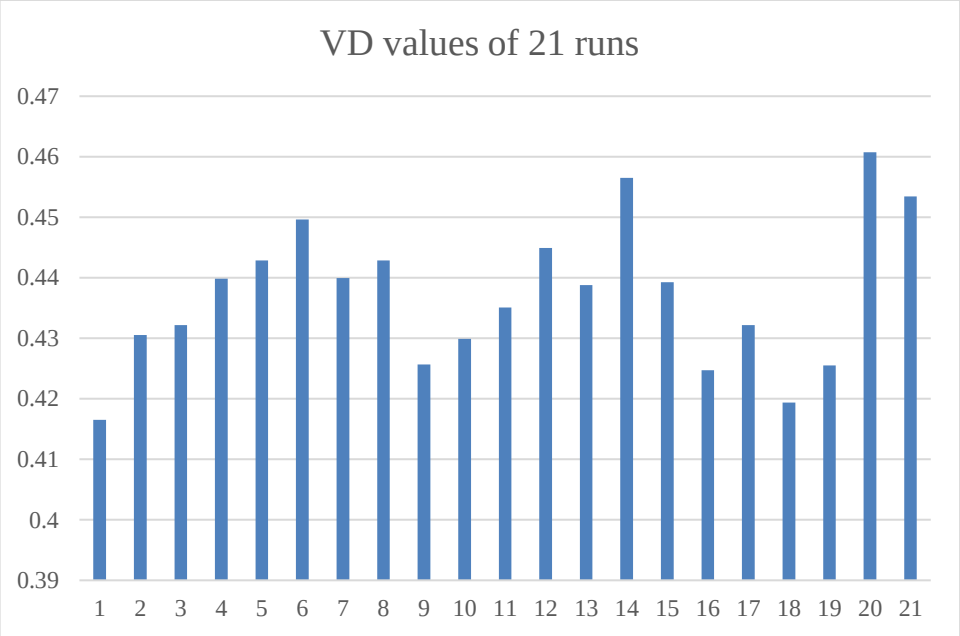

Figure 4.3. VD values for 21 runs of the simulation.

Furthermore, knowing that some of the generators are working near the limitation range of their reactive power, it is essential to have a practical constraint handling method like “constraint domination” which is used in this study. This will assure that while choosing the best solutions, critical points won’t be thrown away with methods like the penalty factor. Figure 4.4 shows the reactive power schedule of generators.

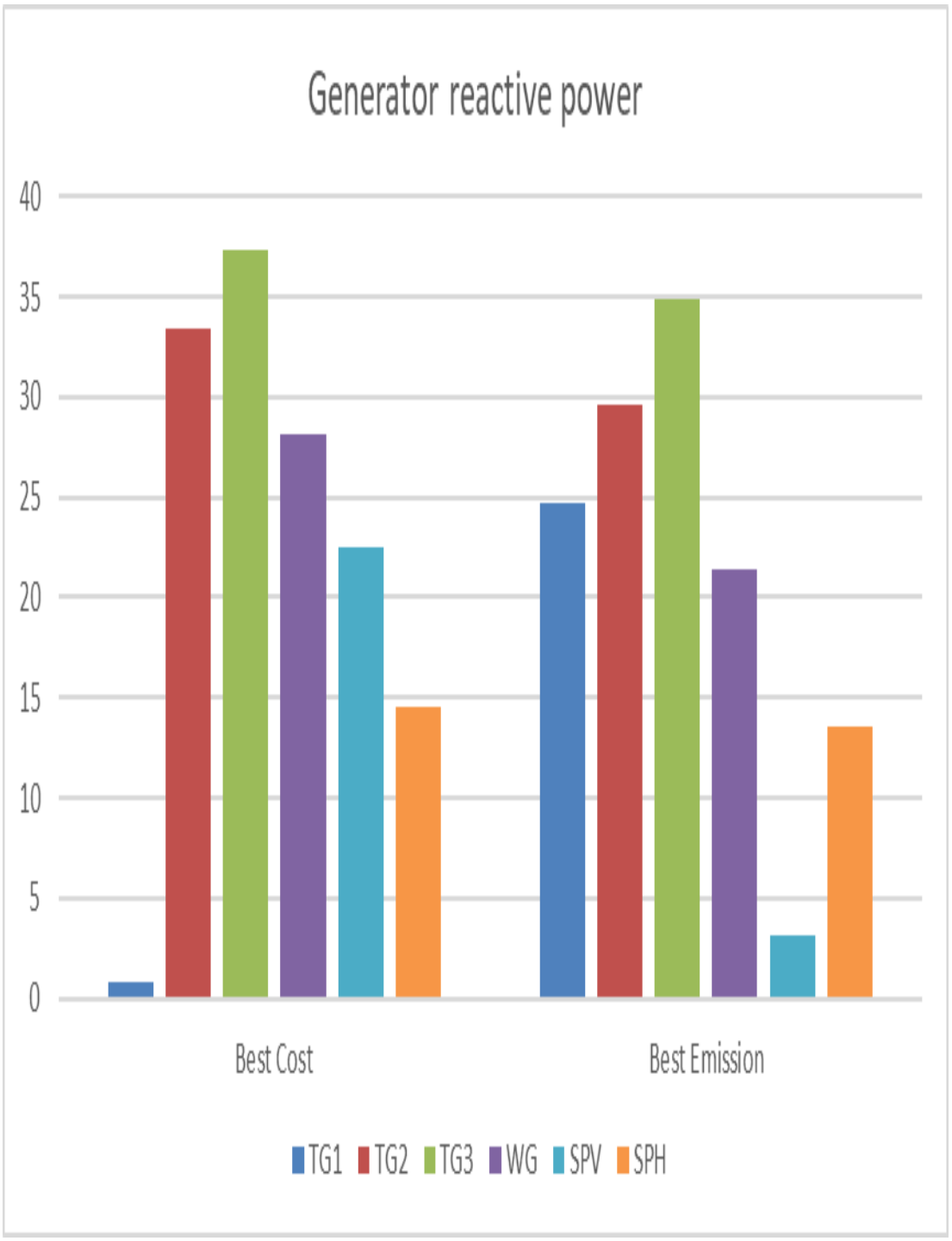

Figure 4.4. Generators reactive power (MVAr).

In the next chapter, conclusion and brief summary of the study are given and possible future work is mentioned.

Chapter 5

CONCLUSION

In this study, an algorithm was developed to find *pareto* fronts of ideal solutions for the problem of multi-objective economic emission power dispatch implemented with stochastic solar, small hydro, and wind units. In the energy section and with the current policies of companies and governments, a study like this becomes more pertinent since consideration of clean energy sources is in order. Well-known and suitable probability density functions for forecasting stochastic behavior of all the renewable energy sources have been used. Prohibited operating zones are incorporated in the design of a thermal unit. The multi-objective R-NSGA-II algorithm is enforced to solve the non-convex and non-linear MOEED problem. An appropriate constraint handling method, "constraint domination" has been integrated with the original multi-objective NSGA-II. All constraints of the system along with the network security restrictions are properly met with the help of the constraint domination method. Detailed investigation of *pareto* fronts using hypervolume indicator, an inspection of fuzzy decision making for solution extraction as well as a comparative review of the outcomes acquired from many experiments of the R-NSGA-II method with two previously studied algorithms are accomplished. Results show that R-NSGA-II outperforms both SMODE-SF as well as MOEA/D-SF in individual comparisons of cost and emission, significantly. The superiority of the R-NSGA-II method was discussed and consistency of the results was shown. The suggested formulation on EED can be studied in future work by using other well-known algorithms like NSGA-III.

REFERENCES

[1] Ustun, T. S., Ozansoy, C., & Zayegh, A. (2011). Recent developments in microgrids and example cases around the world-A review. *Renewable & Sustainable Energy Reviews*, *15*(8), 4030-4041. https://doi.org/10.1016/j.rser.2011.07.033

[2] Planas, E., Gil-De-Muro, A., Andreu, J., Kortabarria, I., & Martínez De Alegría, I. (2013). General aspects, hierarchical controls and droop methods in microgrids: A review. *Renewable and Sustainable Energy Reviews*, *17*, 147-159. https://doi.org/10.1016/j.rser.2012.09.032

[3] Lasseter, B. (2001). Microgrids [distributed power generation]. 2001 IEEE power engineering society winter meeting. Conference proceedings (Cat. No. 01CH37194),

[4] Lasseter, R. H. (2002). Microgrids. 2002 IEEE Power Engineering Society Winter Meeting. Conference Proceedings (Cat. No. 02CH37309),

[5] Bower, W. I., Ton, D. T., Guttromson, R., Glover, S. F., Stamp, J. E., Bhatnagar, D., & Reilly, J. (2014). *The advanced microgrid. Integration and interoperability* (SAND2014-1535; Other: 504877 United States 10.2172/1204100 Other: 504877 SNL English). https://www.osti.gov/servlets/purl/1204100

[6] Morris, G. Y., Abbey, C., Wong, S., & Joos, G. (2012). Evaluation of the costs and benefits of Microgrids with consideration of services beyond energy supply.

[7] Young-Morris, G., Abbey, C., Joos, G., & Marnay, C. (2011). A framework for the evaluation of the cost and benefits of microgrids. *CIGRE 2011 Bologna Symposium - The Electric Power System of the Future: Integrating Supergrids and Microgrids*.

[8] Zhong, J. (2018). *Power System Economic and Market Operations*. CRC Press.

[9] Bhardwaj, A., Vikram Kumar, K., Vijay Kumar, S., Singh, B., & Khurana, P. (2012). Unit commitment in electrical power system-a literature review.

[10] Gaddam, R. R. (2013). Optimal unit commitment using swarm intelligence for secure operation of solar energy integrated smart grid. *Power Systems Research Centre, IIIT Hyderabad*.

[11] Júnior, J. D. A. B., Nunes, M. V. A., Nascimento, M. H. R., Rodríguez, J. L. M., & Leite, J. C. (2018). Solution to economic emission load dispatch by simulated annealing: case study. *Electrical Engineering*, *100*(2), 749-761. https://doi.org/10.1007/s00202-017-0544-0

[12] Zhou, J., Wang, C., Li, Y., Wang, P., Li, C., Lu, P., & Mo, L. (2017). A multi-objective multi-population ant colony optimization for economic emission dispatch considering power system security. *Applied Mathematical Modelling*, *45*, 684-704. https://doi.org/10.1016/j.apm.2017.01.001

[13] Roy, P. K., & Bhui, S. (2016). A multi-objective hybrid evolutionary algorithm for dynamic economic emission load dispatch. *International Transactions on Electrical Energy Systems*, *26*(1), 49-78. https://doi.org/10.1002/etep.2066

[14] Modiri-Delshad, M., Aghay Kaboli, S. H., Taslimi-Renani, E., & Rahim, N. A. (2016). Backtracking search algorithm for solving economic dispatch problems with valve-point effects and multiple fuel options. *Energy*, *116*, 637-649. https://doi.org/10.1016/j.energy.2016.09.140

[15] Júnior, J. D. A. B., Nunes, M. V. A., Nascimento, M. H. R., Leite, J. C., Rodriguez, J. L. M., Freitas, C. A. O. D., Júnior, M. F., Oliveira, E. F. D., Alencar, D. B. D., Moraes, N. M., Carvajal, T. L. R., & Oliveira, H. M. D. (2018). Multi-Objective Optimization Techniques to Solve the Economic Emission Load Dispatch Problem Using Various Heuristic and Metaheuristic Algorithms. In. InTech. https://doi.org/10.5772/intechopen.76666

[16] Adarsh, B. R., Raghunathan, T., Jayabarathi, T., & Yang, X.-S. (2016). Economic dispatch using chaotic bat algorithm. *Energy*, *96*, 666-675. https://doi.org/10.1016/j.energy.2015.12.096

[17] Jayabarathi, T., Raghunathan, T., Adarsh, B. R., & Suganthan, P. N. (2016). Economic dispatch using hybrid grey wolf optimizer. *Energy*, *111*, 630-641. https://doi.org/10.1016/j.energy.2016.05.105

[18] Meng, A., Li, J., & Yin, H. (2016). An efficient crisscross optimization solution to large-scale non-convex economic load dispatch with multiple fuel types and valve-point effects. *Energy*, *113*, 1147-1161. https://doi.org/10.1016/j.energy.2016.07.138

[19] Secui, D. C. (2015). A new modified artificial bee colony algorithm for the

economic dispatch problem. *Energy Conversion and Management, 89*, 43-62. https://doi.org/10.1016/j.enconman.2014.09.034

[20] Gjorgiev, B., & Čepin, M. (2013). A multi-objective optimization based solution for the combined economic-environmental power dispatch problem. *Engineering Applications of Artificial Intelligence*, *26*(1), 417-429. https://doi.org/10.1016/j.engappai.2012.03.002

[21] Zhang, Y., Gong, D.-W., & Ding, Z. (2012). A bare-bones multi-objective particle swarm optimization algorithm for environmental/economic dispatch. *Information Sciences*, *192*, 213-227. https://doi.org/10.1016/j.ins.2011.06.004

[22] Srinivasa Rao, B., & Vaisakh, K. (2013). Multi-objective adaptive Clonal selection algorithm for solving environmental/economic dispatch and OPF problems with load uncertainty. *International Journal of Electrical Power & Energy Systems*, *53*, 390-408. https://doi.org/10.1016/j.ijepes.2013.04.024

[23] Mondal, S., Bhattacharya, A., & Nee Dey, S. H. (2013). Multi-objective economic emission load dispatch solution using gravitational search algorithm and considering wind power penetration. *International Journal of Electrical Power & Energy Systems*, *44*(1), 282-292. https://doi.org/10.1016/j.ijepes.2012.06.049

[24] Yao, F., Dong, Z. Y., Meng, K., Xu, Z., Iu, H. H.-C., & Wong, K. P. (2012). Quantum-Inspired Particle Swarm Optimization for Power System Operations Considering Wind Power Uncertainty and Carbon Tax in Australia. *IEEE Transactions on Industrial Informatics*, *8*(4), 880-888.

https://doi.org/10.1109/tii.2012.2210431

[25] Jadhav, H. T., & Roy, R. (2013). Gbest guided artificial bee colony algorithm for environmental/economic dispatch considering wind power. *Expert Systems with Applications*, *40*(16), 6385-6399. https://doi.org/10.1016/j.eswa.2013.05.048

[26] Abul'Wafa, A. R. (2013). Optimization of economic/emission load dispatch for hybrid generating systems using controlled Elitist NSGA-II. *Electric Power Systems Research*, *105*, 142-151. https://doi.org/10.1016/j.epsr.2013.07.006

[27] Ghasemi, A., Gheydi, M., Golkar, M. J., & Eslami, M. (2016). Modeling of Wind/Environment/Economic Dispatch in power system and solving via an online learning meta-heuristic method. *Applied Soft Computing*, *43*, 454-468. https://doi.org/10.1016/j.asoc.2016.02.046

[28] Qu, B. Y., Liang, J. J., Zhu, Y. S., Wang, Z. Y., & Suganthan, P. N. (2016). Economic emission dispatch problems with stochastic wind power using summation based multi-objective evolutionary algorithm. *Information Sciences*, *351*, 48-66. https://doi.org/10.1016/j.ins.2016.01.081

[29] Zhu, Y., Wang, J., & Qu, B. (2014). Multi-objective economic emission dispatch considering wind power using evolutionary algorithm based on decomposition. *International Journal of Electrical Power & Energy Systems*, *63*, 434-445. https://doi.org/10.1016/j.ijepes.2014.06.027

[30] Azizipanah-Abarghooee, R., Niknam, T., Roosta, A., Malekpour, A. R., & Zare,

M. (2012). Probabilistic multiobjective wind-thermal economic emission dispatch based on point estimated method. *Energy*, *37*(1), 322-335. https://doi.org/10.1016/j.energy.2011.11.023

[31] Khan, N. A., Awan, A. B., Mahmood, A., Razzaq, S., Zafar, A., & Sidhu, G. A. S. (2015). Combined emission economic dispatch of power system including solar photo voltaic generation. *Energy Conversion and Management*, *92*, 82-91. https://doi.org/10.1016/j.enconman.2014.12.029

[32] Kheshti, M., Kang, X., Bie, Z., Jiao, Z., & Wang, X. (2017). An effective Lightning Flash Algorithm solution to large scale non-convex economic dispatch with valve-point and multiple fuel options on generation units. *Energy*, *129*, 1-15. https://doi.org/10.1016/j.energy.2017.04.081

[33] Surender Reddy, S., Bijwe, P. R., & Abhyankar, A. R. (2015). Real-Time Economic Dispatch Considering Renewable Power Generation Variability and Uncertainty Over Scheduling Period. *IEEE Systems Journal*, *9*(4), 1440-1451. https://doi.org/10.1109/jsyst.2014.2325967

[34] Reddy, S. S. (2017). Optimal scheduling of thermal-wind-solar power system with storage. *Renewable Energy*, *101*, 1357-1368. https://doi.org/10.1016/j.renene.2016.10.022

[35] Biswas, P. P., Suganthan, P. N., & Amaratunga, G. A. J. (2017). Optimal power flow solutions incorporating stochastic wind and solar power. *Energy Conversion and Management*, *148*, 1194-1207.

https://doi.org/10.1016/j.enconman.2017.06.071

[36] Liu, G., Zhou, J., Xiao, X., Li, M., Yang, Y., & Lu, C. (2018). Dynamic Economic Dispatch in Thermal-Wind-Small Hydropower Generation System. In (Vol. 246). Les Ulis: EDP Sciences.

[37] Salkuti, S. R. (2020). Multi-objective based economic environmental dispatch with stochastic solar-wind-thermal power system. *International Journal of Electrical & Computer Engineering (2088-8708), 10*(5).

[38] Yalcinoz, T., & Rudion, K. (2020). Multi-objective Environmental-economic Load Dispatch Considering Generator Constraints and Wind Power Using Improved Multi-objective Particle Swarm Optimization. *Advances in Electrical and Computer Engineering*, *20*(4), 3-10.

[39] Li, X., Wang, W., Wang, H., Wu, J., Fan, X., & Xu, Q. (2020). Dynamic environmental economic dispatch of hybrid renewable energy systems based on tradable green certificates. *Energy*, *193*, 116699. https://doi.org/10.1016/j.energy.2019.116699

[40] Biswas, P. P., Suganthan, P. N., Qu, B. Y., & Amaratunga, G. A. J. (2018). Multiobjective economic-environmental power dispatch with stochastic wind-solar-small hydro power. *Energy*, *150*, 1039-1057. https://doi.org/10.1016/j.energy.2018.03.002

[41] Sarda, J., & Pandya, K. (2019, 2019//). Optimal Active–Reactive Power Dispatch

Considering Stochastic Behavior of Wind, Solar and Small-Hydro Generation. Applications of Artificial Intelligence Techniques in Engineering, Singapore.

[42] Sulaiman, M. H., & Mustaffa, Z. (2021). Solving optimal power flow problem with stochastic wind–solar–small hydro power using barnacles mating optimizer. *Control Engineering Practice*, *106*, 104672. https://doi.org/10.1016/j.conengprac.2020.104672

[43] Pandya, S. B., & Jariwala, H. R. (2020). Stochastic Wind-Solar-Small Hydro Power Plant Integrated Multi-Objective Optimal Power Flow Using Multi Verse Optimizer. *Journal of Green Engineering*, *10*, 615-645.

[44] Abdullah, M., Javaid, N., Chand, A., Khan, Z. A., Waqas, M., & Abbas, Z. (2019, 2019//). Multi-objective Optimal Power Flow Using Improved Multi-objective Multi-verse Algorithm. Web, Artificial Intelligence and Network Applications, Cham.

[45] Paish, O. (2002). Small hydro power: technology and current status. *Renewable and Sustainable Energy Reviews*, *6*(6), 537-556.

[46] Rawa, M., Abusorrah, A., Bassi, H., Mekhilef, S., Ali, Z. M., Abdel Aleem, S. H. E., Hasanien, H. M., & Omar, A. I. (2021). Economical-technical-environmental operation of power networks with wind-solar-hydropower generation using analytic hierarchy process and improved grey wolf algorithm. *Ain Shams Engineering Journal*. https://doi.org/10.1016/j.asej.2021.02.004

[47] Wijesinghe, A., & Lai, L. L. (2011). Small hydro power plant analysis and development. 2011 4th International Conference on Electric Utility Deregulation and Restructuring and Power Technologies (DRPT),

[48] Chang, T. P. (2010). Investigation on frequency distribution of global radiation using different probability density functions. *International Journal of Applied Science and Engineering*, *8*(2), 99-107.

[49] Shi, L., Wang, C., Yao, L., Ni, Y., & Bazargan, M. (2011). Optimal power flow solution incorporating wind power. *IEEE Systems Journal*, *6*(2), 233-241.

[50] Mujere, N. (2011). Flood frequency analysis using the Gumbel distribution. *International Journal on Computer Science and Engineering*, *3*(7), 2774-2778.

[51] Cabus, P. (2008). River flow prediction through rainfall–runoff modelling with a probability-distributed model (PDM) in Flanders, Belgium. *Agricultural Water Management*, *95*(7), 859-868.

[52] Zimmerman, R. D., & Murillo-Sánchez, C. E. (2020). *Matpower 7.1*. In *https://matpower.org* Available: https://zenodo.org/record/4074135

[53] Biswas, P. P., Suganthan, P. N., Mallipeddi, R., & Amaratunga, G. A. (2018). Optimal power flow solutions using differential evolution algorithm integrated with effective constraint handling techniques. *Engineering Applications of Artificial Intelligence*, *68*, 81-100.

[54] Dubey, H. M., Pandit, M., & Panigrahi, B. (2015). Hybrid flower pollination algorithm with time-varying fuzzy selection mechanism for wind integrated multi-objective dynamic economic dispatch. *Renewable Energy, 83*, 188-202.

[55] Powell, D., & Skolnick, M. M. (1993). Using genetic algorithms in engineering design optimization with non-linear constraints. Proceedings of the 5th International conference on Genetic Algorithms,

[56] Deb, K. (2000). An efficient constraint handling method for genetic algorithms. *Computer methods in applied mechanics and engineering*, *186*(2-4), 311-338.

[57] Deb, K. (2011). Multi-objective optimisation using evolutionary algorithms: an introduction. In *Multi-objective evolutionary optimisation for product design and manufacturing* (pp. 3-34). Springer.

[58] Kramer, O. (2017). Genetic algorithms. In *Genetic algorithm essentials* (pp. 11-19). Springer.

[59] Mitchell, M. (1998). *An introduction to genetic algorithms*. MIT press.

[60] Starkweather, T., McDaniel, S., Whitley, C., Mathias, K., Whitley, D., & Dept, M. (2002). A Comparison of Genetic Sequencing Operators.

[61] Whitley, D., & Starkweather, T. (1990). Genitor II: A distributed genetic algorithm. *Journal of Experimental & Theoretical Artificial Intelligence*, *2*(3), 189-214.

[62] Whitley, D., Starkweather, T., & Shaner, D. (1991). *The traveling salesman and sequence scheduling: Quality solutions using genetic edge recombination*. Citeseer.

[63] Deb, K., & Agrawal, R. B. (1995). Simulated binary crossover for continuous search space. *Complex systems*, *9*(2), 115-148.

[64] Deb, K., & Agrawal, S. (1999). A niched-penalty approach for constraint handling in genetic algorithms. Artificial Neural Nets and Genetic Algorithms,

[65] Larranaga, P., Kuijpers, C. M., Murga, R. H., & Yurramendi, Y. (1996). Learning Bayesian network structures by searching for the best ordering with genetic algorithms. *IEEE transactions on systems, man, and cybernetics-part A: systems and humans*, *26*(4), 487-493.

[66] Deb, K., & Goyal, M. (1996). A combined genetic adaptive search (GeneAS) for engineering design. *Computer Science and informatics*, *26*, 30-45.

[67] Srinivas, N., & Deb, K. (1994). Muiltiobjective optimization using nondominated sorting in genetic algorithms. *Evolutionary computation*, *2*(3), 221-248.

[68] Goldberg, D. E., Korb, B., & Deb, K. (1989). Messy genetic algorithms: Motivation, analysis, and first results. *Complex systems*, *3*(5), 493-530.

[69] Schaffer, J. D. (1984). *Some experiments in machine learning using vector evaluated genetic algorithms (artificial intelligence, optimization, adaptation, pattern recognition)* Vanderbilt University].

[70] Deb, K., Pratap, A., Agarwal, S., & Meyarivan, T. (2002). A fast and elitist multiobjective genetic algorithm: NSGA-II. *IEEE transactions on evolutionary computation*, *6*(2), 182-197.

[71] While, L., Hingston, P., Barone, L., & Huband, S. (2006). A faster algorithm for calculating hypervolume. *IEEE transactions on evolutionary computation*, *10*(1), 29-38.

[72] Bringmann, K., & Friedrich, T. (2013). Approximation quality of the hypervolume indicator. *Artificial Intelligence*, *195*, 265-290.

APPENDICES

Appendix A: Load Data

Table A.1. Load data for IEEE 30-bus system

Bus No.	Load (100%) MW	Load (100%) MVAr	Bus No.	Load (100%) MW	Load (100%) MVAr
1	0	0	16	3.5	1.8
2	21.7	12.7	17	9	5.8
3	2.4	1.2	18	3.2	0.9
4	7.6	1.6	19	9.5	3.4
5	94.2	19	20	2.2	0.7
6	0	0	21	17.5	11.2
7	22.8	10.9	22	0	0
8	30	30	23	3.2	1.6
9	0	0	24	8.7	6.7
10	5.8	2	25	0	0
11	0	0	26	3.5	2.3
12	11.2	7.5	27	0	0
13	0	0	28	0	0
14	6.2	1.6	29	2.4	0.9
15	8.2	2.5	30	10.6	1.9
Total load: **283.4** MW, **126.2** MVAr					

Appendix B: Branch Data

Table B.1. Branch data for IEEE 30-bus system

Branch no.	Bus No.		R (p.u.)	X (p.u.)	B (total) (p.u.)	Rating (MVA)	Branch no.	Bus No.		R (p.u.)	X (p.u.)	B (total) (p.u.)	Rating (MVA)
	From	To						From	To				
1	1	2	0.0192	0.0575	0.0264	130	22	15	18	0.1070	0.2185	0	16
2	1	3	0.0452	0.1852	0.0204	130	23	18	19	0.0639	0.1292	0	16
3	2	4	0.0570	0.1737	0.0184	65	24	19	20	0.0340	0.0680	0	32
4	3	4	0.0132	0.0379	0.0042	130	25	10	20	0.0936	0.2090	0	32
5	2	5	0.0472	0.1983	0.0209	130	26	10	17	0.0324	0.0845	0	32
6	2	6	0.0581	0.1763	0.0187	65	27	10	21	0.0348	0.0749	0	32
7	4	6	0.0119	0.0414	0.0045	90	28	10	22	0.0727	0.1499	0	32
8	5	7	0.0460	0.1160	0.0102	70	29	21	22	0.0116	0.0236	0	32
9	6	7	0.0267	0.0820	0.0085	130	30	15	23	0.1000	0.2020	0	16
10	6	8	0.0120	0.0420	0.0045	32	31	22	24	0.1150	0.1790	0	16
11	6	9	0	0.2080	0	65	32	23	24	0.1320	0.2700	0	16
12	6	10	0	0.5560	0	32	33	24	25	0.1885	0.3292	0	16
13	9	11	0	0.2080	0	65	34	25	26	0.2544	0.3800	0	16
14	9	10	0	0.1100	0	65	35	25	27	0.1093	0.2087	0	16
15	4	12	0	0.2560	0	65	36	28	27	0	0.3960	0	65
16	12	13	0	0.1400	0	65	37	27	29	0.2198	0.4153	0	16
17	12	14	0.1231	0.2559	0	32	38	27	30	0.3202	0.6027	0	16
18	12	15	0.0662	0.1304	0	32	39	29	30	0.2399	0.4533	0	16
19	12	16	0.0945	0.1987	0	32	40	8	28	0.0636	0.2000	0.0214	32
20	14	15	0.2210	0.1997	0	16	41	6	28	0.0169	0.0599	0.0065	32
21	16	17	0.0824	0.1932	0	16							